The Mixture Formation Process In The Radial Engine

Politechnika Lubelska
Wydział Mechaniczny
ul. Nadbystrzycka 36
20-618 LUBLIN

Konrad Pietrykowski
Mirosław Wendeker

The Mixture Formation Process In The Radial Engine

Politechnika Lubelska
Lublin 2010

Recenzent: prof. dr hab. inż. Jacek Nowakowski, prof. Akademii Techniczno-Humanistycznej w Bielsku-Białej

Redakcja i skład: Konrad Pietrykowski

Publikacja wydana za zgodą Rektora Politechniki Lubelskiej

ISBN: 978-83-62596-09-6

Wydawca: Politechnika Lubelska
ul. Nadbystrzycka 38D, 20-618 Lublin
Realizacja: Biblioteka Politechniki Lubelskiej
Ośrodek ds. Wydawnictw i Biblioteki Cyfrowej
ul. Nadbystrzycka 36A, 20-618 Lublin
tel. (81) 538-46-59, email: wydawca@pollub.pl
www.biblioteka.pollub.pl
Druk: Wydawnictwo-Drukarnia „Liber Duo"
ul. Długa 5, 20-346 Lublin

Preface

The keynote of this monograph is the authors belief that the position of an intake pipe of each cylinder in a radial engine significantly affects the mixture formation in a cylinder. If these differences are taken into account in an algorithm to control multi-point fuel injection, the cycle-to-cycle variations of individual cylinders will be reduced.

The aim of the monograph is to describe an algorithm to control injection time in a radial engine under transient conditions that includes varied mixture formation in individual cylinders.

This monograph proves, that there is a significant effect of the geometric orientation of inlet pipes in radial engines on the parameters typical of mixture formation.

The scope of the monograph includes:

- the analysis of the-state-of-the-art on the mixture formation in inlet pipes in gasoline engines,
- the analysis of the-state-of-the-art on the cycle-to-cycle variations of a working process in radial engines,
- the construction of a test stand,
- the experimental study on a radial engine,
- the analysis of the research results attained,
- developing a control algorithm for fuel injection in radial engines,
- work evaluation.

The analysis of the state-of-the-art gives rise to the following conclusions:

- the cycle-to-cycle variability of a working process in radial engines has been confirmed experimentally,
- the cycle-to-cycle variations are determined primarily by varied mixture composition in cylinders,
- the non-uniform distribution of fuel film in each inlet pipe may be one of the reasons,
- there is no evidence in the literature on the impact of the geometric orientation of a cylinder axis on film motion,
- the simulation studies demonstrated that the geometric orientation of a cylinder axis influences the state of film in an inlet pipe,
- to unify mixture composition in individual cylinders, it is necessary to re-place a carburetor with a multi-point injection system,
- the doses of fuel injected into intake pipes should be differentiated properly, especially in a transient state.

It is necessary to conduct tests to determine the differences in the mixture formation in individual cylinders in a radial engine and their underlying causes. The best solution is experimental research. This is due to the insufficient data on the temperature distribution in an inlet pipe, the impact of roughness on the behavior of fuel film and other factors.

Research assumptions

The research object was a 9-cylinder radial engine ASz-62IR. This type of an engine was chosen as the monographs authors participated in the research project which was financed by the Polish Ministry of Science and Information Technology “The development and implementation of an electronic system to control the operation of a powerful aviation piston engine K9-E” (no. 03605/CT12-6/2005). As a result, there was designed a multi-point injection gasoline system in a radial engine that was controlled electronically. In addition, an engine with the injection system was tested. The results attained were used to calibrate the fuel injection control system.

The testing was carried out on a single copy of an engine under assumed operating conditions defined by constant crankshaft speed and constant pressure in an inlet pipe. This was due to extra-merits reasons, i.e. engine testing in an aviation test bench was expensive and its time was limited. Besides, it is sufficient to confirm the hypothesis advanced (that such an impact exists) for selected operating conditions. If the hypothesis had been difficult to prove, the testing under other conditions or on any other copy of the engine should be repeated. Crankshaft rotational speed was 1770 rpm and load pressure was 94 kPa. These conditions correspond to engine cruising speed and are the most common during operation.

There was a test of significance on the mean values of the coefficient typical of mixture formation. It determines the number of operation cycles after stroke injection timing until mixture composition in a cylinder becomes settled. This coefficient was determined by the experimental research that consisted of a stroke-like change of a fuel dose injected into the next cylinder. The maximum pressure in a cylinder was analyzed. Based on the literature, it was noted that maximum pressure is the best factor out of the information provided by measuring indicated pressure to assess mixture composition.

Does the arrangement of cylinders in radial engines influence the formation and disappearance of fuel film in these engines?

Konrad Pietrykowski
Mirosław Wendeker

Lublin, 25.10.2010

1. Aircraft piston combustion engines

Piston combustion engines have been used in aviation since it started. They are a large group of aviation propulsion systems. In spite of the intensive development of jet or turbine engines, they are frequently used in small recreation and sports planes, and farming, cargo and fire extinguishing planes This is due to their cheap maintenance, low flight speed and relatively easy operation.

This monograph is devoted to the radial engines with cylinders mounted radially around a crankshaft which is connected only to one crank. A master rod connects a piston of the first cylinder and a crankshaft. Other rods are not linked directly with a crankshaft, but the master rod. Radial engines are usually 3, 5, 7 or 9-cylinder engines as a single star although they can also have up to four circles of cylinders. To ensure regular speed, ignition takes place subsequently in every second cylinder. Two-stroke diesel engines with an even number of cylinders were rarely produced. A radial engine is fitted with a charging compressor to provide the proper amount of air during flight at high altitude. This is usually a radial compressor that is driven by a crankshaft through a multiplying gear. Air moves from a compressor diffuser to cylinders through individual inlet pipes. Most radial engines are fuelled with a carburetor although some can have a mechanical fuel injection system. Two spark plugs per cylinder and a dual ignition coil provide reliable ignition. Most piston aircraft engines are air cooled, which is due to the efforts to minimize airframe weight.

The main advantages of radial engines compared with turbine and row piston engines are given below. The characteristics of the engine that make these advantages are in parentheses.

The advantages of radial engines:

- a compact design (a crankshaft with one crank),
- low weight (air cooled),
- fast response to load changes (multi-cylinder engines, no flywheel),
- its weight is 15% less compared to an in-line engine of the same power (compact design),
- low cost of purchase, operation and repair (simple design),
- lower fuel consumption compared with turbine engines (higher efficiency),
- better cooling compared with in-line engines (large frontal area),
- simple overhauls and easy maintenance (simple design),
- high reliability (simple design),
- they work even a cylinder is damaged (air cooled).

Thanks to these advantages, radial engines are still developed. Producers research into how to enhance their power, to improve their efficiency and to reduce their vibration. The main disadvantages of radial engines in relation to turbine ones are lower power and high air resistance during flight due to their large front surface. Another disadvantage concerns a dispersion of an ignition angle in each cylinder, which is caused by a design of a crankshaft system. While using radial engines, it is necessary to remember to drain lubricating oil which accumulates in engine inlet pipes and to lower cylinder heads after a long shutdown. If this procedure is neglected, connecting rods may be damaged. Another drawback of the design is varied mixture composition in individual cylinder, which causes cycle-to-cycle variations.

A study concentrates just on how to improve engine smoothness. Different orientation of cylinders against the vertical affects mixture composition and consequently the process of combustion in each cylinder. This follows from the fact that inlet pipes that connect a compressor and heads are identical in shape but they provide an air-fuel mixture of varied composition. This is probably the effect of gravity on oil droplets and fuel film. Upper cylinders are supplied with a lean mixture, whereas lower with a rich one. As a lean mixture burns longer, the temperature of components around a combustion chamber increases excessively. It is difficult to keep a proper head temperature in radial air-cooled engines. Such conditions are conducive to engine knocking. To prevent this, a head temperature is lowered and a mixture is enriched. Then, when upper cylinders are supplied with appropriate mixture composition, the lower ones receive a too rich mixture, which leads to increased fuel consumption.

Cycle-to-cycle variability of individual cylinders in a single cycle is typical of all multi-cylinder engines. Combustion and the performance of a successive cylinder are influenced by:

- a shape of an inlet system [12], [72], [16],
- a design of a combustion chamber [4] and piston-shaft system,
- mixture mass and composition, its stratification [26], turbulence intensity and its scale, the share of residual gases [39], [44], the degree of atomization and fuel evaporation, etc.,
- combustion initiation and its course [71], i.e. spark, the development of a flame kernel and its front, flame quenching on walls, etc.,
- a cylinder thermal state.

If the values of the above factors are non-uniform for individual cylinders, there are cycle-to-cycle variations [35]. This is typical of carburettor engines where fuel is supplied in a single-point way [10]. Non-uniform mixture formation within an air stream that flows through an inlet pipe and its unequal distribution among the cylinders [8], [54] alters the composition and temperature of residual gases and the temperature of cylinder walls, which even increases cycle-to-cycle variations. Cycle-to-cycle variability in individual cylinders also influences the unrepeatability of the working process in each cylinder (variability in successive engine cycles). The reasons for the unrepeatability of combustion include [5], [37]:

- varied mixture distribution in a cylinder due to the inaccurate mixing of fuel, air and residual gases,
- location and size of a vortex where spark occurs,
- stochastic nature of floating a spark kernel from a spark plug gap to the remained area of a combustion chamber,
- varied intensity and turbulence,
- unrepeatable characteristics of spark discharges.

At idle, unrepeatability is even up to 40% of torque produced [43]. In addition, it is highly influenced by the phenomenon of "misfiring" (unwanted lack of combustion). According to the study by Piernikarski [40] misfire at idle occurred in more than 1.5% of cycles.

The solution to this problem can be multi-point injection. Consequently, it is possible to stabilize mixture composition in a steady state. Mixture composition varies in a transient state [60] in petrol engines with indirect injection. This follows a lag in fuel transportation, and the appearance and disappearance of fuel film on inlet pipe walls.

The phenomenon of fuel film has been researched intensively for the past twenty years. It has been found that the process of fuel film formation and reduction is influenced the most by factors such as:

- temperature of air, fuel, intake pipe and valve,
- frequency of successive injections,
- type of fuel,
- injector design and the way it is mounted in an intake pipe,
- intensity and direction of air flow,
- pressure in an inlet system.

It should be emphasized that the study to explain dynamic phenomena when mixture is formed were carried out on automotive engines. Their inlet pipes are positioned against gravity in an identical manner. Radial engines are of a specific design. Their intake system is different from that of in-line engines (Figure 1.1). A carburetor, depending on an engine type, is placed above or below a crankshaft. A mixture flows through a carburetor base into a radial compressor inlet (in super-charged engines) that is mounted asymmetrically. Later, it is compressed and flows through inlet pipes to cylinders. The way cylinders are arranged makes a mixture move in accordance with (lower cylinders) or opposite to (upper cylinder) the direction of gravity. Fuel film occurs in the engines in which a mixture is formed in an inlet system. The way fuel film is transported may depend on gravity. Thus, the following issue needs to be explored:

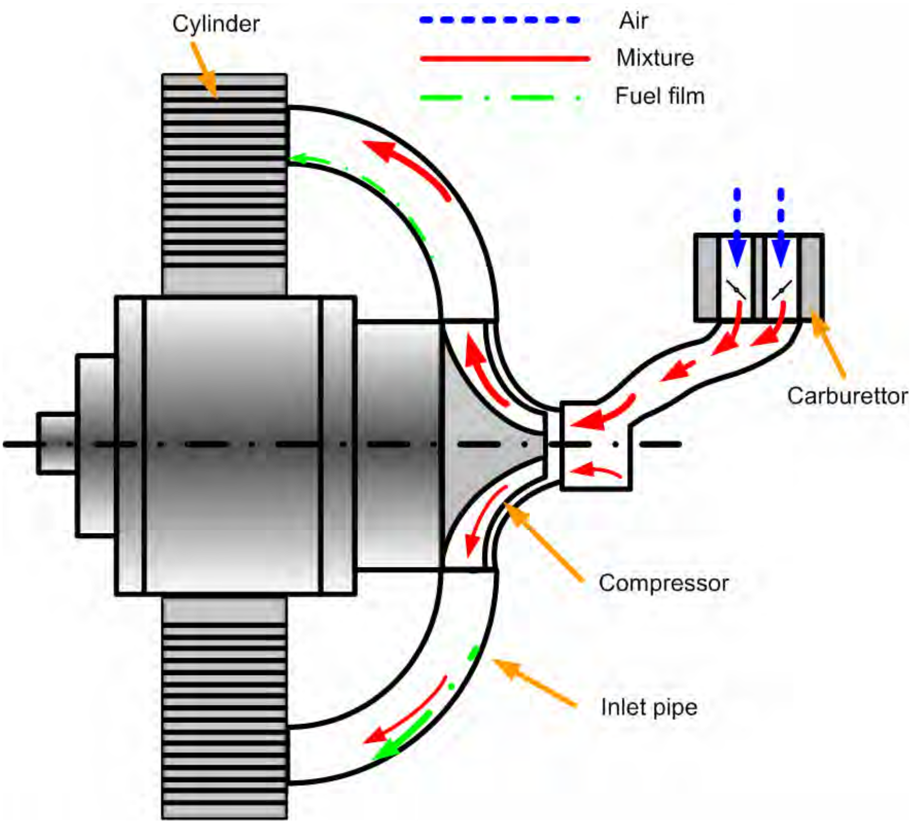

Fig. 1.1. Diagram of an inlet system in a radial engine

2. Non-uniform mixture composition in radial engines

Despite the production of radial engines was reduced in recent years, they still are very popular. The research to improve their design is continued. Radial Engines Ltd. can be a good example. The company produces a 7-cylinder radial engine - Jacobs R755 of a maximum power of 205 kW. Its first version was powered with a Bendix Stromberg precipitation carburettor that was mounted below an engine axis. An air-fuel mixture was supplied from the carburetor into the cylinders through the channel as a cast engine block and then through the steel tubes to the cylinder heads. Based on the studies, it was noted that the Jacobs like other radial engines of a similar design has the varied temperature of cylinder heads and of exhaust gas in individual cylinders [78]. The distribution of exhaust gas temperature in each cylinder in the Jacobs R755 is given in Figure 2.2.

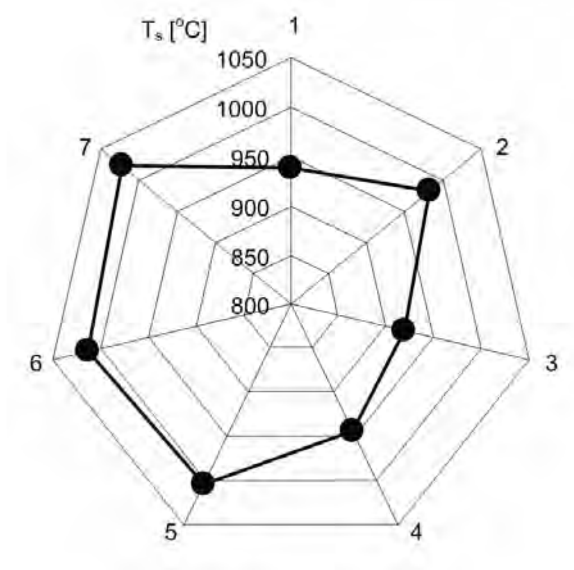

Fig. 2.2. Exhaust gas temperature Ts for the individual cylinders in the JACOBS R755B2 (cruising power, n = 2000 rpm, h = 600 m above sea level, maximally lean mixture) [78]

Based on the data, it can be concluded that non-uniform mixture composition causes varied exhaust gas temperature. The temperature of the exhaust gas in cylinder 7 (leanest mixture) is about 110 ºC higher than the one in cylinder 3 (richest mixture). When the mean mixture composition is stoichiometric, the 7th cylinder gets the leanest mixture. If the mean mixture composition that fuels the cylinders is enriched, the temperature of the exhaust gas in the 7th cylinder drops. The other cylinders, however, are fuelled by an over-enriched mixture. A rich mixture gives rise to the following problems:

- Higher fuel consumption. An excessively enriched mixture in some cylinders lowers combustion efficiency.
- Non-uniform power generated by individual cylinders. If only the 7th cylinder is fuelled by an optimally composed mixture, it will be the only cylinder that generates maximum power. Cylinder 7 can generate power around 31 kW, whereas cylinder 3 fuelled by an over-enriched mixture can generate only 25 kW.
- High vibration of the engine. By applying multipoint fuel injection, vibration significantly decreased.
- Carbon deposits on exhaust valves. This is the most serious effect of engine operation if some cylinders work with a too rich mixture. For 22 years, the cases of the excessive deposition of carbon and lead on valves and valve seats have been observed. This reduces compression cylinders. In almost all cases, this problem occurs in the cylinders that are fuelled by an over-enriched mixture. The exhaust gas temperature is not high enough to burn off the accumulated deposition.

These factors lead us to consider the use of fuel injection as an opportunity to improve the performance of the Jacobs engine (and other radial engines.) In 2001, Radial Engines Ltd. started to certify an injection system in a standard aviation category. They decided to use a serial injection system Bendix RSA10 mounted in aircraft engines. The injector nozzles by GAMI were chosen to compensate exhaust gas temperature in individual cylinders. These nozzles inject fuel directly into inlet valve seats through modified inlet pipes. The engine drives a main fuel pump and pre-pump which ensures a required fuel pressure (0.18 MPa) before starting the engine. Little modification to an engine or airframe is necessary to install the sys-tem.

The following results have been achieved when the power system in the Jacobs was modified:

- temperature of exhaust gas and power of individual cylinders are more similar,
- higher engine power,
- no tendency to lead and soot deposits on sockets and exhaust valves,
- lower fuel consumption.

Polish producers also work to improve the properties of radial engines. WSK “PZL Kalisz” S.A. produces a 9-cylinder radial engine ASz-92IR. It is a carburretor-powered engine. Its maximum power is 745 kW. Based on the measurements of engine head temperature, it was found that there may be nonuniform mixture distribution between cylinders. In 2005, an electronically controlled gasoline injection system was constructed in cooperation with Lublin University of Technology thanks to the research project financed by the Polish Ministry of Science and Higher Education.

The preliminary research was carried out in cooperation with the author of the monograph and confirmed the cycle-to-cycle variability of individual cylinders [9]. The phenomenon is the most intensive at low speed (Figure 2.3), which is supported by the literature [22]. The covariance of maximum pressure is several times higher than for speed above 1200 rpm.

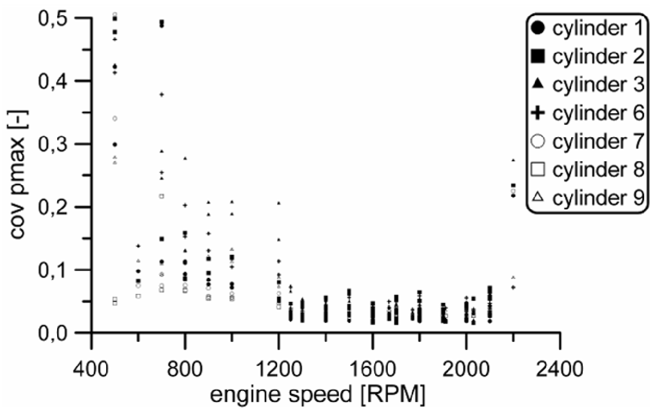

Fig. 2.3. Covariance of the maximum pressure in the cylinders in relation to rotational speed [9]

Cycle-to-cycle variations can be noted in the time courses of cylinder pressure (Figure 2.4). The non-uniform mixture composition causes the differences in the combustion process. Thus, while the combustion in cylinder 8 is proper, the mixture composition in cylinder 3 is at a flammability limit.

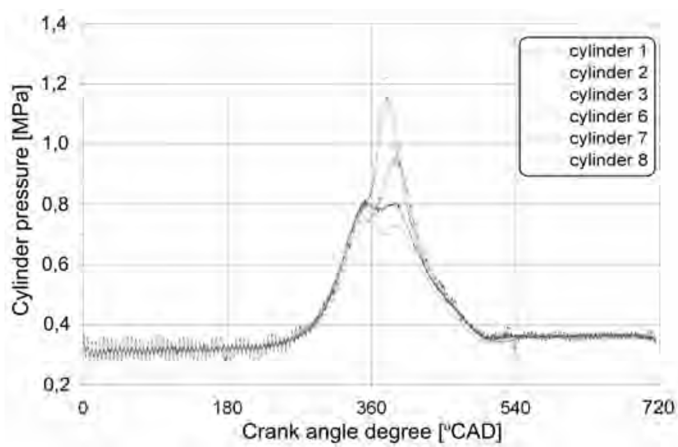

Fig. 2.4. Time course of the cylinder pressure in ASz-62IR (800 rpm speed and 52 kPa charging pressure [9]

3. Phenomena accompanying gasoline injection

Fuel in the inlet system in carburretor-based engines with a single-point and multi-point injection is as atomized droplets in the air, a layer of fuel film on walls and fuel vapor mixed with air [1], [3], [10], [20], [21], [32]. While forming a mixture, there are the following processes [58]:

- formation and development of a fuel stream injected,
- deposition of fuel droplets on walls of a throttle, intake pipe and intake valves,
- lifting of fuel droplets by an air stream,
- fuel evaporation (out of droplets and fuel film),
- dripping of fuel into a cylinder caused by gravity and air pressure on fuel film.

It has long been known that transient conditions significantly influence mixture composition in a cylinder, especially in single-point injected engines as the distance and time to mixed fuel and air are longer there [60]. To test this phenomenon, they use a test in which a throttle is opened in a jump-like manner, and simultaneously, the pressure in a cylinder [55] and exhaust gas emissions [23] are measured. The sharp increase in load results in the rapid depletion of a mixture, followed by a slow setting of its composition. To diminish this problem, the mixture needs to be temporarily enriched. By sudden closing of the throttle, the mixture composition is temporarily enriched. The examples of the results of such tests are given below (Figure 3.1) [23].

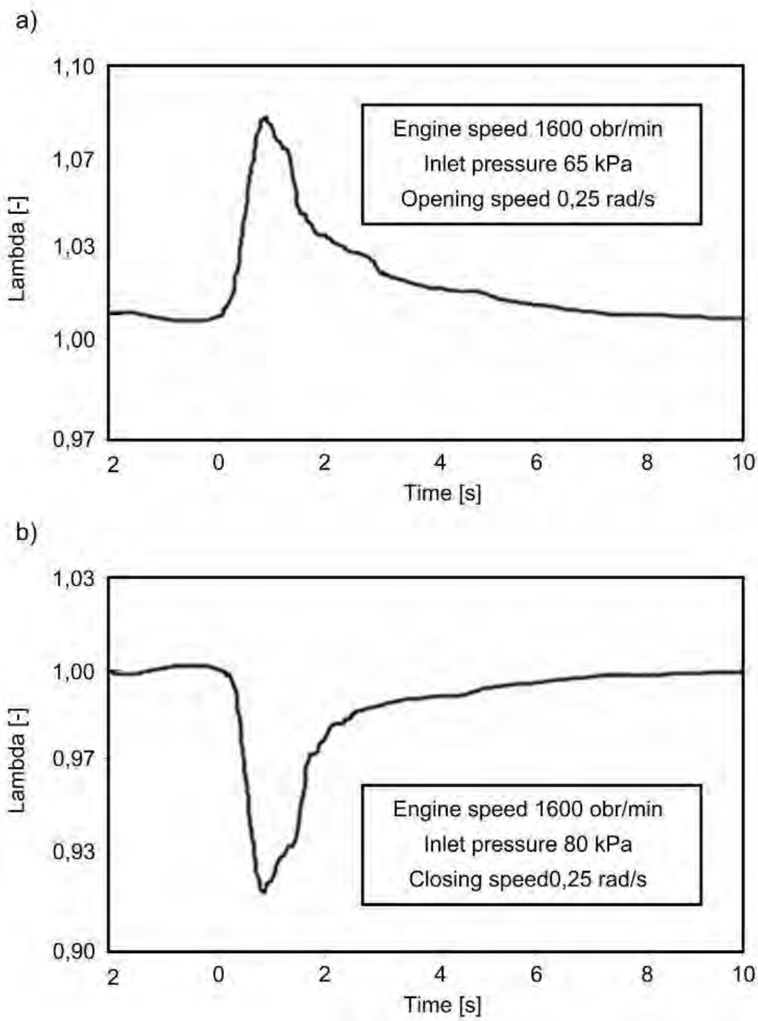

Fig. 3.1. Change of mixture composition when the throttle moves. Carburetor-based engine. A typical effect for: a) a rapid opening of a throttle, b) a rapid closing of a throttle [23]

Both in a steady and transient state, the scheme of the phenomena in an inlet system may undergo as it is shown in Figure 3.2. In a steady state, fuel that is injected in a liquid phase is atomized and transferred in accordance with an air movement. There is atomization, evaporation, collisions, and combination of drop-lets. These droplets settle on the surface of the throttle, intake pipe, intake valve and cylinder to form fuel film.

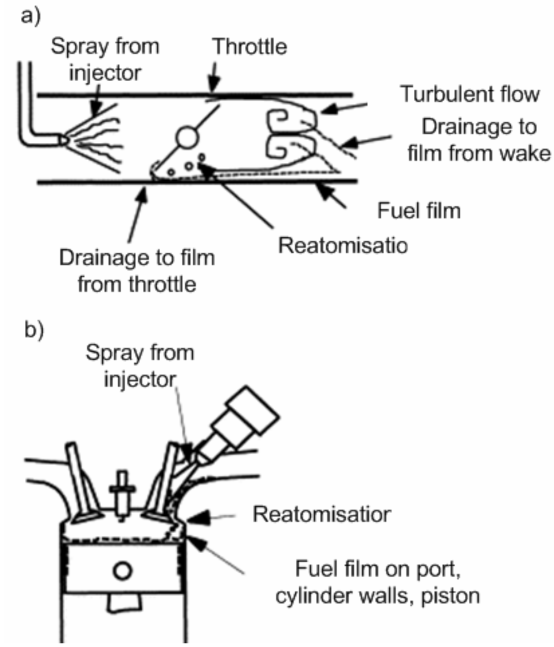

Fig. 3.2. An example of the mixture flow and film formation in an inlet system (a) and a cylinder (b) [2]

Fuel film is transported in accordance with in the direction of air flow, but at a slower speed. Its speed depends on the conditions in an inlet pipe (such as speed, pressure and air temperature, surface roughness) [47], [51], and may be even 100 times smaller than the speed of air flow (Figure 3.3) [2].

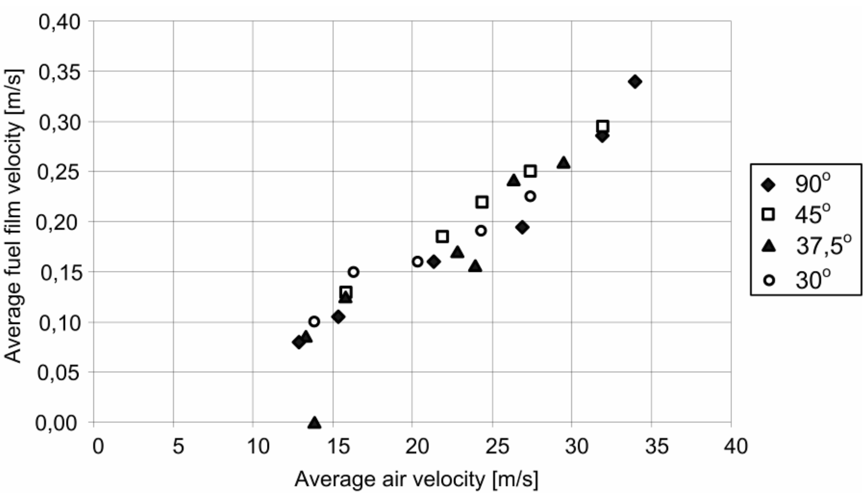

Fig. 3.3. Mean fuel film speed in relation to mean air speed in a straight pipe of a circular section [2]

By rapid opening of the throttle, a fuel deposition scale in fuel film increases and an air-fuel mixture depletes. There is a delay between the time to transport air and the time to transport fuel into a cylinder. In the case of multi-point injection, such a delay is less than that in single-point injected engines. However, it always occurs there. When engine load is reduced, fuel film becomes thinner and air stream becomes richer in fuel. When a throttle moves rapidly [48], delays may vary slightly around the same value, depending on whether it is opened or closed.

It is impossible to observe directly the phenomena described so and not to disturb them. Many studies that describe the phenomena associated with fuel film in a mathematical manner concentrate only on the relationships that come from a physical analysis and do not identify coefficients obtained in experimental research [6], [28], [29], [33] in a test stand. A study on the phenomenon of fuel deposition and its subsequent evaporation is carried out in institutions that deal with engine control algorithms. However, the literature usually provides the examples of the results of such research as coefficients that multiply injection time, depending on a coolant temperature and speed [3].

To analyse the phenomena that occur when mixture is formed, a variety of research methods is applied. Hasson and Flint [17] investigated the degree of deposition of droplets as fuel film on an intake pipe wall. The speed fuel film moves is measured, e.g. by wire sensors [24]. A technical characteristic of an injector has a strong impact on the concentration of fuel vapor and an initial layer of fuel film. The works [67], [11] described such an effect using an analysis of infrared absorption. The same researchers also adopted the technique of Doppler interferometry. They noted that an injector characteristic influences the way fuel is supplied into an intake valve and a range of diameters of fuel droplets that return from an intake valve after being re-atomized. The tested injectors included both classical and air-assisted experimental. Other researchers [64] discovered that pintle injectors under certain conditions can produce a conical stream of too poor droplet atomization. Fuel film is formed more intensively under these conditions. Using the techniques of quick shooting [14], it was found that a valve in engines with a canopy combustion chamber is wetted much. Air injection in air-assisted injectors reduces a droplet diameter and fuel film mass in a combustion chamber. However, there are small areas on a piston crown that are still covered with fuel film. In some combustion chambers, it was noted that fuel film remains on walls until the end of combustion and then is removed along with the exhaust gas and does not take part combustion.

Those methods relate to the analysis of the mixture formation in an inlet system. This process makes some fuel mass remain in a cylinder after an intake valve is closed. Although the fuel in a cylinder is as vapor, droplets and film, a mixture is the most influential on combustion due to the total weight of the fuel in the cylinder. Research into the instantaneous mixture composition in a cylinder are the subject of many papers [7], [36], [38], [45], [63]. They describe measurement methods such as:

- acoustic resonance,
- measurement of ionized exhaust gas,
- measurement of cylinder pressure and load temperature changes,
- measurement of exhaust gas temperature,
- using an oxygen sensor based on zirconium oxide.

To determine mixture composition, different measurement systems were used. One of the easiest ways is to measure it with a wide band lambda sensor LSU mounted in an engine exhaust system. Despite its high measurement accuracy, this method is not useful for measuring the mixture composition in successive cycles. This is due to a significant measurement delay (a few cycles) and the measurement of averaged values of gas composition based on several cycles [56], [61]. The methods to assess the mixture composition in a cylinder in each cycle included the measurement of working gas pressure [15], the composition of the sample of exhaust gas sucked out of a cylinder [73], optoelectronic systems [41], [50], [62], the measurement of ionization in a combustion chamber [13], [34], [42]. The simplest and the most efficient of them is the one based on measuring cylinder pressure.

4. Model of the mixture formation

In literature, there is no physical model, i.e. only-theory-based, of the phenomena associated with fuel film in an inlet system. Ongoing research is aimed at making a model of heat and mass transfer in fuel film, and it deals with direct fuel injection into a combustion chamber, e.g. Santon [52], [53] and Yoshikawa [70]. They describe how an injector design can influence exhaust gas emissions and diesel engine performance. Therefore, there is a need to conduct an experimental study to identify the coefficients in an experimental model.

In an experimental model, it is assumed that part of fuel injected into an inlet pipe enters a cylinder as droplets, and the rest is supplemented by fuel film. The speed fuel evaporates from fuel film is proportional to its mass. It also depends on an evaporation time constant which is a function of engine operating conditions. The time constant is mainly influenced by the speed of the air flow and pressure in an inlet system. Fuel evaporation from film and pushing film into a cylinder come together and simplify a mathematical model. Such an approach makes also easier to identify model coefficients experimentally. Considering mixture composition, it does not matter how this mixture reaches a cylinder because it is assumed that fuel that gets there will evaporate immediately. These findings can be described mathematically as follows [58]:

$$m_c = m_w \cdot (x-1) + m_f \cdot \frac{\tau}{\Delta t} \tag{4.1}$$

where:

- m_c - the mass of the fuel in a cylinder,
- m_w - the total mass of the fuel injected by an injector during its opening,
- m_f - the mass of the fuel in fuel film on inlet system walls,
- x - the coefficient of deposition of the fuel injected on inlet system walls,
- $\tau/\Delta t$ - the percentage of fuel film mass taken together with air as liquid, and evaporated,
- τ - fuel evaporation time constant,
- Δt - the interval between successive cycles of injections.

Based on the literature, air speed in an inlet system, rotational speed and the amount of fuel injected are the most influential on fuel film parameters. During the tests involving the rapid movement of a throttle, the intensity fuel film is formed and reduced would be a function of time. Such an experiment could have a big logical error. Similarly, it would be in the case of a significant change in rotational speed. A method of a stroke-like change in the mass of fuel injected at a constant speed and pressure in an inlet system gives the best results.

In the available literature, fuel film is described in detail. However, the impact of gravity on its behavior in an engine inlet pipe is not investigated at all.

Model tests using CFD (Computational Fluid Dynamics) were carried out to deal with this issue. CFD modeling enables a quick analysis of complex flow phenomena, and stand tests would be very expensive here. There are certain papers that prove this method to be useful for analyzing fuel film transportation. Milton [32], Senda [46] and Lan et al [30] conducted model tests with the use of ANSYS FLUENT software to check the impact of air speed on the thickness and range of water film. The results show that as the speed of air flow increases, fuel film thickness decreases and its area expands. The experimental verification using an interferometer confirmed the results of the calculations.

The objective of the model tests was to determine how gravity influences the motion of the fuel film inside an inlet pipe in a radial engine. The testing was done using STAR-CD software by CD-adapco [76]. It simulates fluid flow by means of CFD. The program uses the Navier - Stokes equations and the energy conservation laws. STAR-CD is applied in industry and research [75]. It also has modules necessary to simulate the phenomena that occur in combustion engines.

The geometry of the model was based on the dimensions of the intake pipe in the engine tested. The model was cylindrical. It was 600 mm long and 62 mm in diameter. Its volume was discretized into 6000 elements (Figure 4.1). Air was assumed to be a flowing agent; and its density depended on pressure and temperature.

The models of k-Epsilon turbulence and fuel film were adopted. They took into account gravity, too. It was assumed that at an initial instant the walls are covered partially with fuel film 0.2 mm thick (Figure 4.2), which was based on the studies by Lee and Cheng [31] and Hayashi and Sawa [19]. They used a conductive sensor and obtained a value of 0.05 - 0.2 mm. The value of 0.2 mm was adopted due to the relatively low temperature of the intake pipe walls in the engine tested, a significant surface roughness and a large distance between the injector and the inlet valve. Pressure, speed and temperature were selected on the basis of the specification provided by the ASz-62IR manufacturer. The values adopted were for mean speeds and loads. The values adopted for model boundary conditions were as follows:

- constant flow speed in the inlet section 7 m/s,
- constant air pressure in the outlet section 60 kPa,
- film thickness 0.2 mm,
- temperature of the cooling agent and walls 60 °C.

In order to test the impact of the location of the pipe towards the vertical, the two cases with two different directions of air flow were investigated.

A calculation step was 0.02 s. This value is a compromise between calculation time and calculation stability. One second was simulation time as the results are the most legible then. Shorter time would diminish the differences in fuel film distribution, whereas for longer time fuel film would begin to flow through the outlet section. The calculations for a single case lasted about 4 minutes.

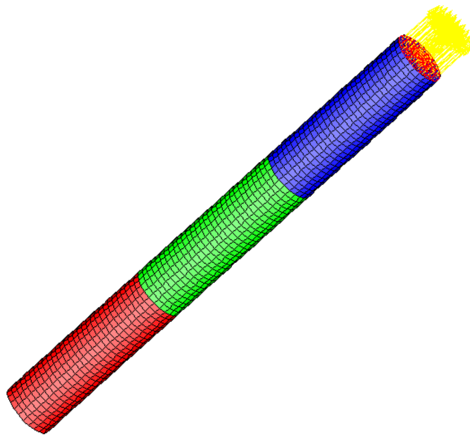

Fig. 4.1. Computational mesh

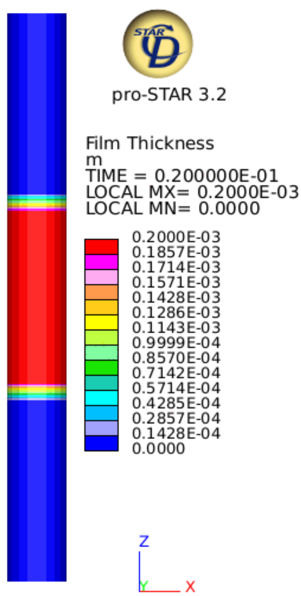

Fig. 4.2. Initial film thickness

The distributions of fuel film thickness and film speed were as follows: the maximum film thickness reduced to 0.191 and the film speed reached 0.9 m/s for upward movement (Figure 4.3). For downward movement, the fuel film extended to a larger area reaching a maximum thickness of 0.176 mm and a maximum speed of 0.19 m/s. In both cases, the motion of the film was in the direction of gravity.

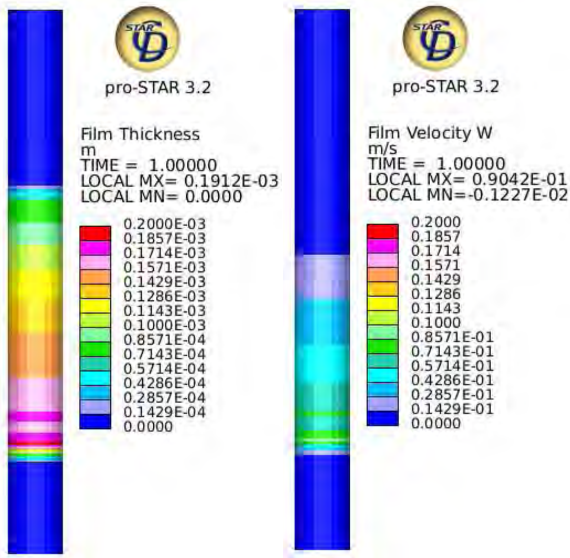

Fig. 4.3. Thickness and speed of the fuel film if air flows up

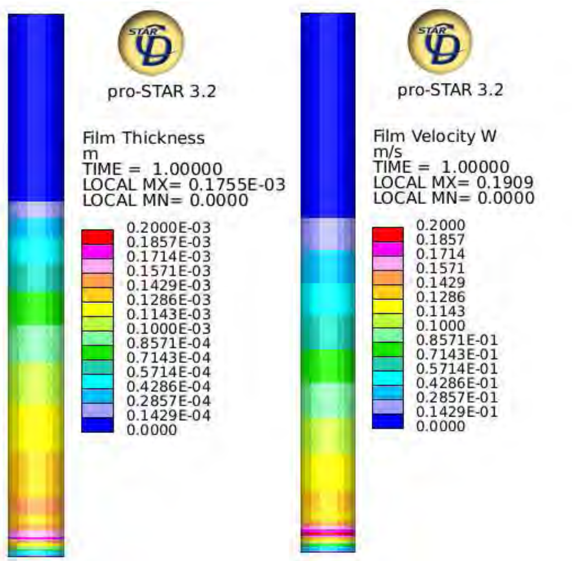

Fig. 4.4. Thickness and speed of the fuel film if air flows down

As noted in the research, gravity influences the motion of film inside an inlet pipe in a radial engine. The film flows downwards both in the upper and lower intake pipes. It follows that gravity helps film motion in the pipes of lower cylinders and prevents it in the pipes of upper cylinders.

5. Experimental setup

5.1 Introduction

This section describes the test stand. The description of the research laboratory provides the information about its location, possible control and monitoring engine operation, the operation of its measurement and executive systems. Additionally, there is the technical characteristic of the object tested and the description of the changes that were introduced in the engine design, especially in its mechatronic injection system. The chapter deals with the structure and operation of the system with respect to mechanics, electronics (control unit) and IT that allows a user to communicate with the system. The additional measurement systems to attain the research objective were also described.

5.2 Test bench

The stand testing was performed in the engine test house at WSK PZL Kalisz. The stand is designed to conduct research into aircraft piston engines of high power. It consists of an engine room, a control room and a room with fuel and oil installations. An engine mounted on a construction to measure torque (Figures 5.1 and 5.2) is in the engine room.

Channels to ensure free air flow are in the front and rear walls of the control room. They are equipped with steering wheels to direct properly flowing air (Figure 5.2). A fire protection system is mounted on the side and top walls. In case of fire, the engine room is filled with carbon dioxide.

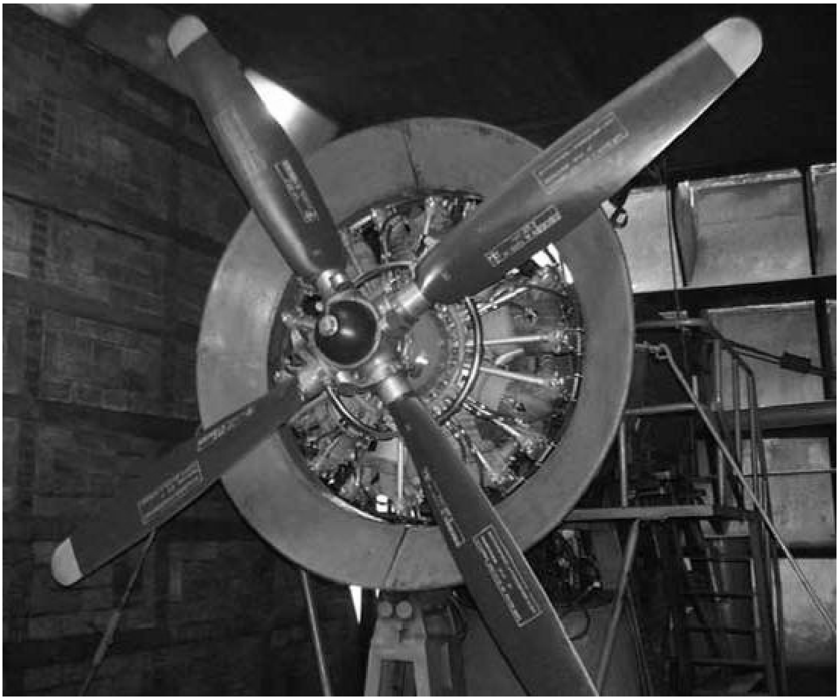

Fig. 5.1. Engine with a propeller on a test stand

Fig. 5.2. Test stand. The view of the measurement system to measure torque, and air guide

A four-blade propeller PZL-SP.OO works as engine load. The load can be altered by adjusting the angle of blade attack. The angle is adjusted by a centrifugal propeller speed regulator R-9SM2 controlled with a lever in the control room. The propeller regulator is to maintain the assumed propeller speed. Engine load can be changed by changing the pressure load in the inlet pipes due to changing the position of a throttle with a lever in a control room. Torque is measured by determining response time in the swinging engine bed. At the test stand, it is possible to measure head temperature using thermocouples under ignition plugs and the temperature of air flowing into the engine. Crankshaft speed is measured with a tachometric generator connected directly to a fuel pump shaft. Pressure is measured with a load compressor pressure gauge.

An adjacent room holds the devices for measuring fuel consumption and lubricating oil supplied to the engine. In the test stand, by changing the temperature of oil flowing through an engine block, its temperature can be changed. Oil consumption is measured using an oil scale. This fuel consumption measurement system is volume-based. Hourly fuel consumption is calculated according to the capacity of tanks, measurement time and fuel temperature. The control room is supplied with the systems to supervise and control the operation of an engine, brake, and other systems (Figure 5.3).

Fig. 5.3. Control room – inside. Control devices and gauges

Reading and recording the values of extremely low frequency is done by hand according to the indications provided by analog indicators. The measurement results are recorded in the test records (Figure 5.4).

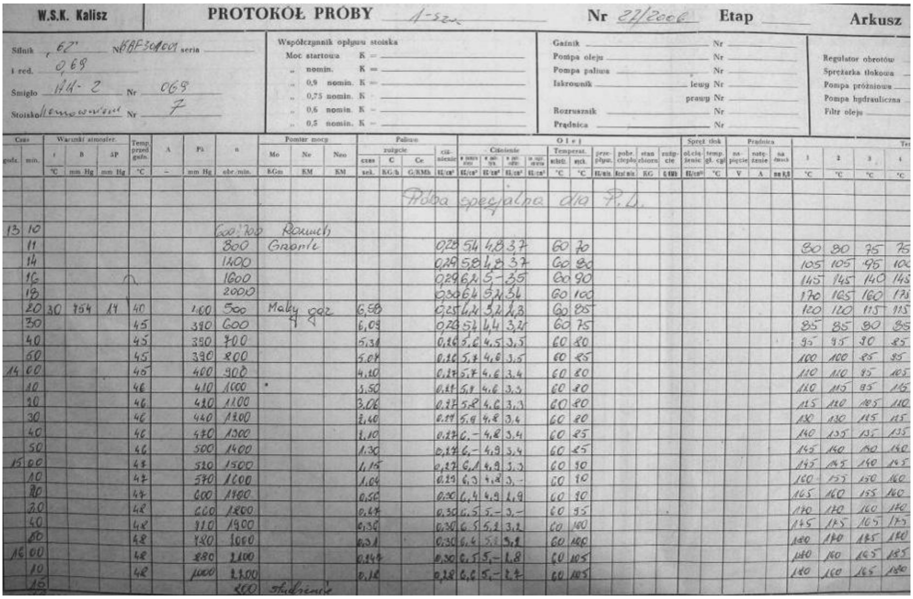
W.S.K. Kalisz | PROTOKÓŁ PRÓBY | Nr 22/2006 | Etap | Arkusz

Silnik | seria | Śmigło | Nr | Stoisko | Nr

Współczynnik oplywu stoiska | Moc startowa K = | nomin. K = | 0,9 nomin. K = | 0,75 nomin. K = | 0,6 nomin. K = | 0,5 nomin. K =

Gaźnik Nr | Pompa oleju Nr | Pompa paliwa Nr | Iskrownik lewy Nr prawy Nr | Rozrusznik Nr | Prądnica Nr

Regulator obrotów | Sprężarka tłokowa | Pompa próżniowa | Pompa hydrauliczna | Filtr oleju

Próba specjalna dla P.L.

Fig. 5.4. Test record

The control room is equipped with the indicators to read the following quantities:

- crankshaft rotational speed,
- compressor charging pressure,
- engine torque,
- temperature of engine heads,
- temperature of air entering the engine,
- fuel consumption,
- oil consumption.

Table 5.1. Accuracy of the instruments in the control room

Quantity	**Accuracy**	**Unit**
Crankshaft rotational speed,	10	rpm
Compressor charging pressure	~1333 (10)	Pa (mmHg)
Engine torque	~9,81 (1)	Nm (kGm)
Temperature of engine heads	5	ºC
Temperature of air entering the engine	1	ºC
Time to measure fuel and oil consumption	0,01	s
Fuel consumption	0,001	dm3
Oil consumption.	10	g

5.3 Research object

The object to test was the ASz-62IR aircraft engine (Figure 5.5) which is an air-cooled, four-stroke and gasoline engine. The engine has nine cylinders arranged in a radial layout [68]. It is supercharged mechanically by a crankshaft driven radial compressor using a multiplying gear of a ratio of 1:8.3. Total cylinder stroke capacity and compression ratio are 29.87 dm3 and 6.4:1, respectively. Maximum power (take-off power) is around 745 kW (1000 hp) at 2200 rpm. Then, the engine has a maximum fuel consumption of about 300 kg/h. The ASz-62IR performance is shown in Table 5.2.

Table 5.2. ASz-62IR performance

Engine power type	**Power Neo**	**Crankshaft rotational speed n**	**Charging pressure Pk**	**Fuel consumption per unit ge**	**Altitude above sea level H**
	[kW]	**[rpm]**	**[kPa]**	**[g/kWh]**	**[m]**
Take-off	745	2200 ±10	140 ±3,3	min. 408	0
Nominal	603	2100 ±10	120 ±1,3	381 ÷ 408	0
Nominal (at nominal altitude)	627	2100 ±10	120 ±1,3	381 ÷ 408	1500
0,9 of nominal power	543	2030 ±10	141 ±2,0	354 ÷ 381	0
0,75 of nominal power	452	1910 ±10	99 ±2,0	326 ÷ 347	0
0,6 of nominal power	362	1770 ±10	89 ±2,0	292 ÷ 320	0
0,5 of nominal power	302	1670 ±10	82 ±2,0	292 ÷ 313	0
Idle	-	500	~45	-	-

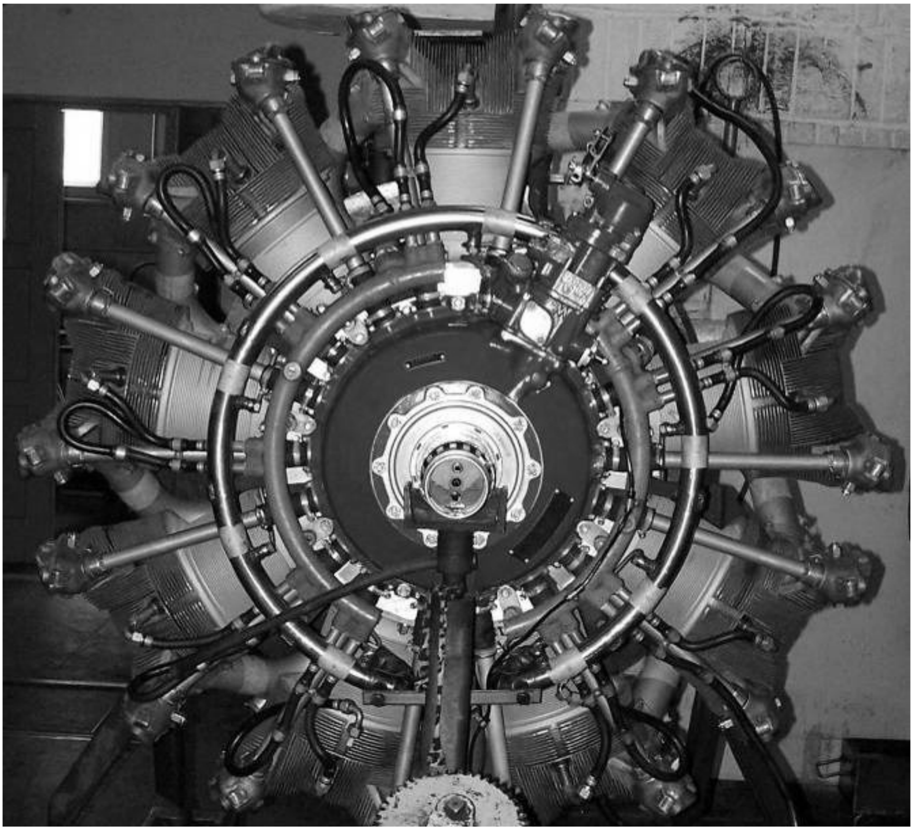

Fig. 5.5. Engine ASz-62IR

The engine was fuelled originally by 100LL aviation fuel by means of a four-carburetor AKM-62IR AVGAS. The carburetor supplied the inlet system with air-fuel emulsion. Ignition is provided by two independent ignition systems. They consist of two magnetoes BSM-PF and eighteen spark plugs SD-48BSM (two spark plugs per cylinder). Spark is at 20 º and 15 º before TDC. The engine is equipped with an electric inertia starter RIM-U-24IR.

In order to do the testing, the supply system was modified and a carburettor was replaced with sequential fuel injection.

5.4 Description of the mechatronic injection system

The engine was fitted with the injectors that supplied fuel to the cylinder inlets. To ensure the mass of injected fuel to be uniform, the injectors were connected to a torus-like fuel battery of a capacity of about 2 dm3 mounted between the propeller and cylinders by steel cables. The battery is not a full torus because at the splitting there are: a fuel input and a fuel pressure regulator with the KTY 19-6M/Z temperature sensor by Infineon (Figure 5.21) and the MPX5700 fuel pressure sensor by Motorola (Figure 5.19). The diagram of the fuel supply system is given in Figure 5.6.

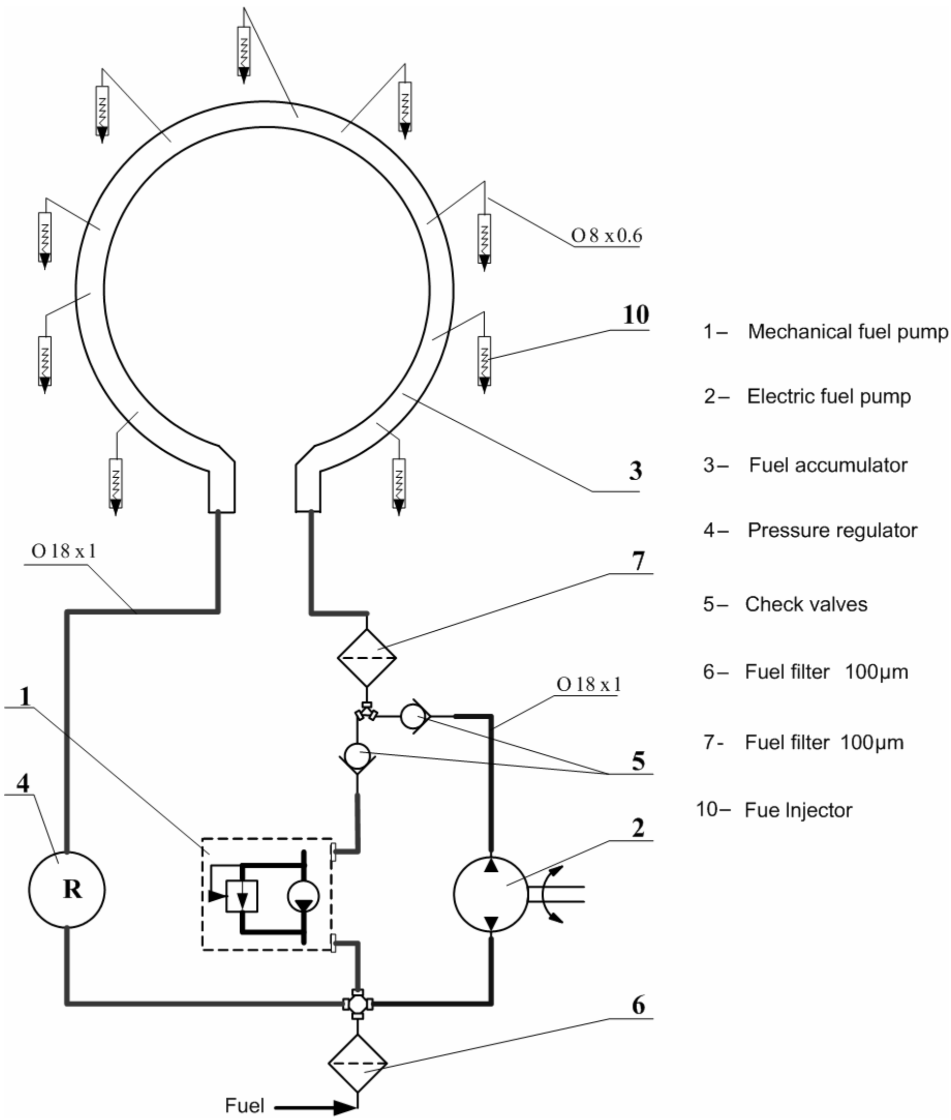

Fig. 5.6. Scheme of the fuel supply system

A fuel pressure regulator P/N 13113 by Aeromotive (Figure 5.7) maintains a constant pressure of 0.3 MPa in relation to compressor pressure. A scapular fuel pump BNK-12BK (Figure 5.8) mounted in a standard manner on the engine was properly adjusted to ensure an adequate flow and fuel pressure. A proper fuel pressure during a take-off is provided with the 11104 Eliminator electric fuel pump by Aeromotive (Figure 5.9) that is supplied with 12 - 13.5 V. The maximum flow of pumped fuel is 180 cm^3/s with a maximum pressure of 0.69 MPa.

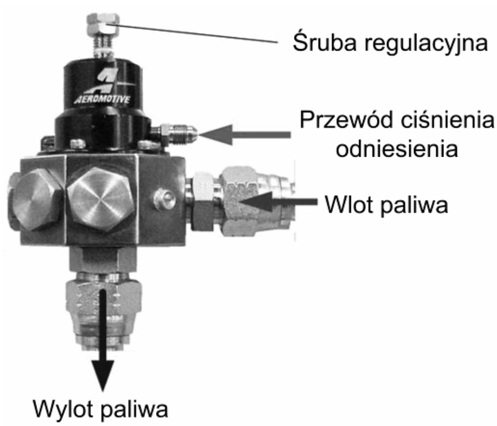

Fig. 5.7. P/N 13113 fuel pressure regulator

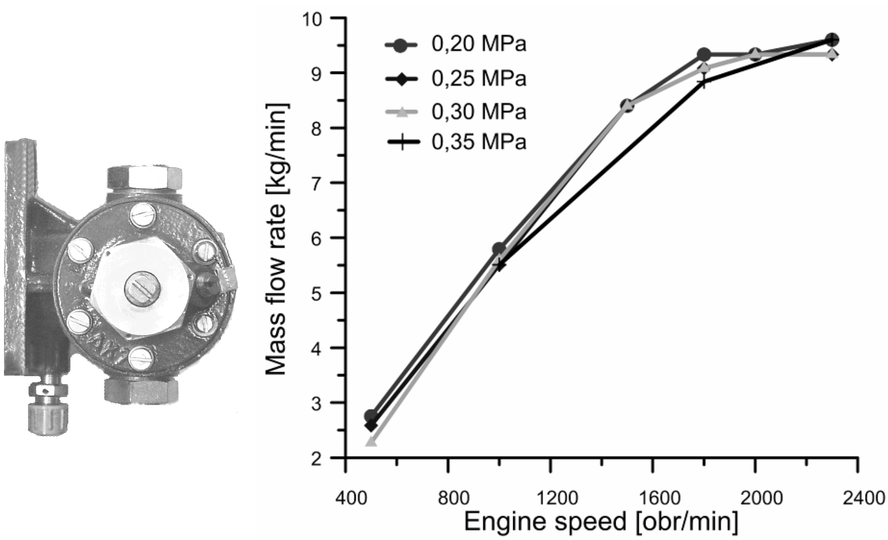

Fig. 5.8. BNK-12BK fuel pump and its characteristic (according to authors research)

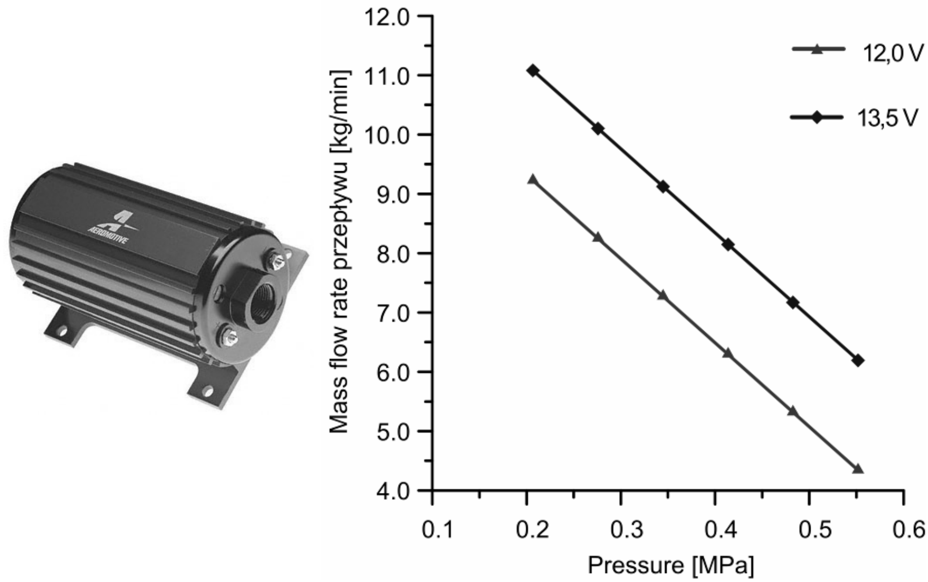

Fig. 5.9. Eliminator fuel pump and its characteristic (according to authors research)

Fuel is supplied to the engine inlet via the Bosch 0280150846 pintle injectors (Figure 5.10) with a maximum efficiency of 1600 cm3/min (pressure of 0.3 MPa). Their resistance is 4.5 Ω, and they are controlled according to a pick and hold system. The arrangement of the injection system elements is shown in Figure 5.11.

Fig. 5.10. Bosch fuel injector

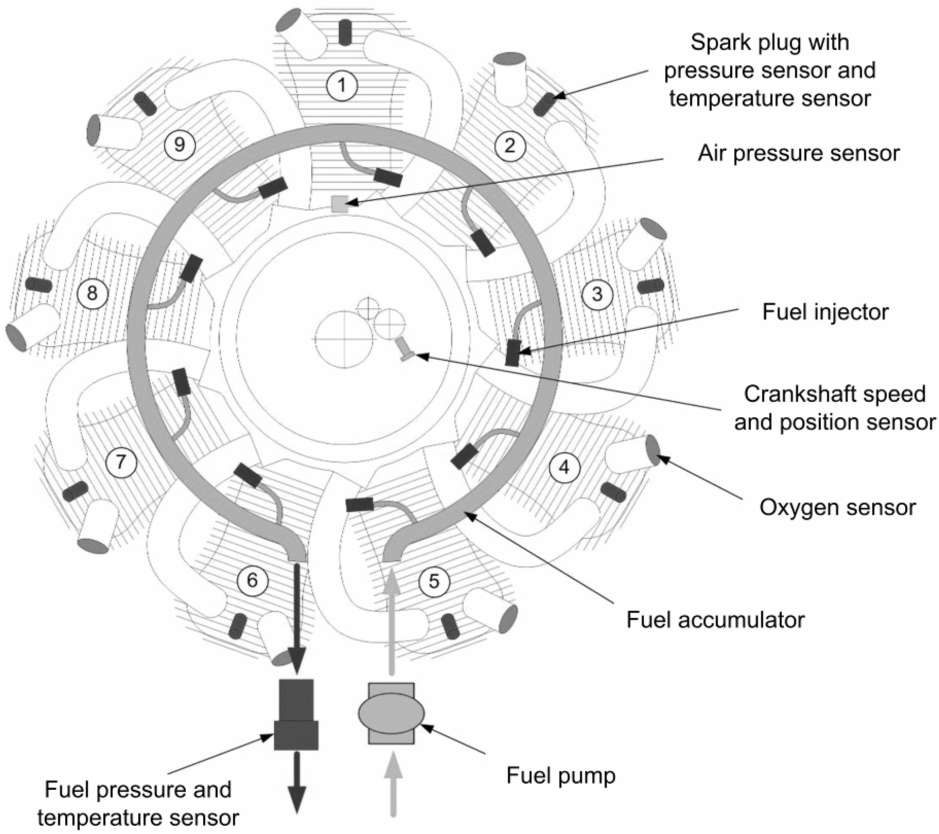

Fig. 5.11. Arrangement of the injection system elements

The operation of the injection system was controlled with a research electronic control unit (Figure 5.12). It was equipped with the RS-232 interfaces that allowed engine operation to be controlled with a PC. It was possible to read and record the following quick-changing quantities thanks to the sensors connected to the control unit (Figure 3.13):

- crankshaft rotational speed,
- crankshaft position,
- the temperature in the intake pipes,
- fuel temperature,
- the pressure in the intake pipe,
- fuel pressure.

The following quantities can be controlled with the control unit:

- opening time of each injector,
- the moment to the electric fuel pump was switched on and off.

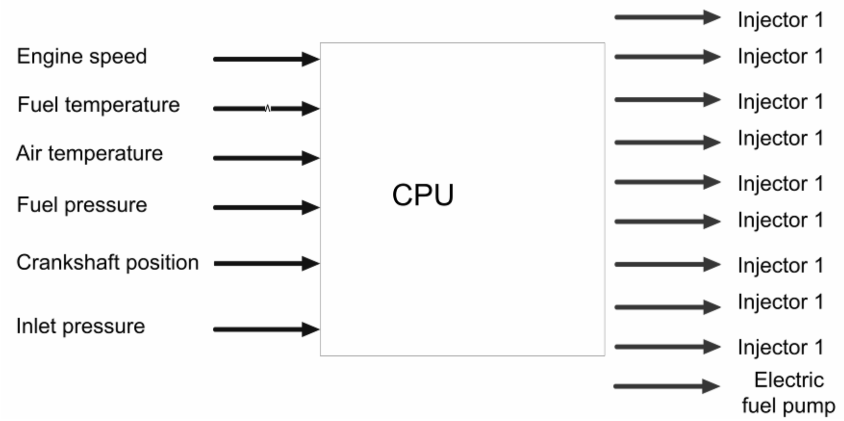

Fig. 5.12. Performance scheme of the control unit

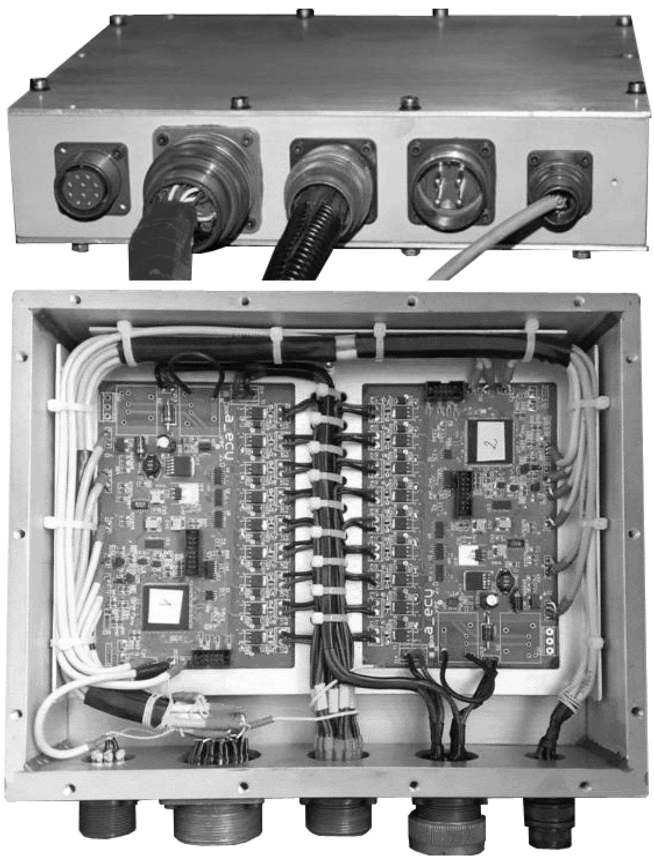

Fig. 5.13. Control unit in the ASz-62IR aviation engine

The control unit allowed the assumed research projects to be attained. The principle of its operation is based on the continuous exchange of information between the control unit and a PC. Consequently, the time to carry out research is shortened a lot and the probability of errors when the next operation cycle is tested is minimized. It is also possible to control the operation of the injection system imposed by characteristics and algorithms developed. Table 5.3 includes the key specifications of the injection control system.

Table 5.3. Specifications of the control system for gasoline injection in ASz-62IR

No.	Description	Value
1.	nominal voltage	24 V
2.	maximum voltage range	22 ÷ 26 V
3.	maximum current input	8,5 A
4.	ambient temperature range	–40 °C to +120 °C
6.	degree of protection	IP66

For safety reasons, the control device consists of two identical control units (Figure 5.13). Both of them operate in parallel to calculate injector opening time according to the indications of sensors and software recorded, but only one of them controls the injectors. In the event the control device fails, the first control unit is switched off and the second one takes over its functions.

The control unit was made as two packages, one of which is an autonomous and universal processor control unit with all necessary support systems, while the second has specialized peripheral systems to maintain appropriate cooperation with the implementing parts, and sensors to control sequential gas injection. A block diagram of this control system is shown in Figure 5.14.

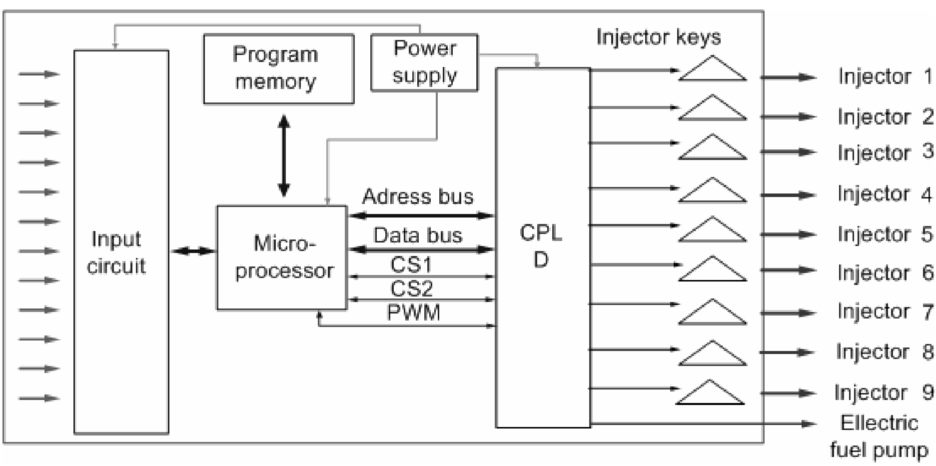

Fig. 3.14. Block diagram of the control system

The control unit was based on a digital signal processor TMS 320 from Texas Instruments. Its design has been developed specially to be suitable for industrial automation control systems. The microcontroller has inside the following functional blocks:

- a 16-bit arithmetic logical unit of a registering structure that allows fundamental operations to be done directly on the content of external memory cells indicated,
- an 8-channel, 10-bit analog-digital transducer,
- a high-speed inputs and outputs system (HSIO) to record changes in input lines and control output lines in real time with an accuracy of 1.6 s,
- a dual-channel video port for data transfering,
- hardware meters which can control the operation of the HSIO systems,
- meters/a software clock to count the intervals set,
- a developed interrupt generation system to respond rapidly to specific types of events,
- a 16-bit watchdog timer that controls the project to be carried out properly and initiates the processor in case of interference.

The block of input circuits consists of a set of elements to convert the signals that come from the sensors mounted on the engine into the logic signals of 0 - 3.3 V because only such a range of voltage is used inside the microprocessor due to the lowest possible energy consumption by the control unit.

The block of input circuits consists of the following parts:

- a rotational speed circuit – a speed sensor generates a discrete voltage signal of 0 - 10 V which is converted to a signal of 0 - 3.3 V and then under-goes optical separation. Noise is filtered (it occurs due to fast switching over as the effect of inducing electric current).
- a pressure sensor circuit – a voltage analogue signal of the sensor has a range of 0 - 5 V, without optical separation. A buffer amplifier reduces voltage in proportion.
- a pressure sensor circuit – a voltage signal is transmitted into the buffer amplifier where it is processed into a range of 0 - 3.3 V.
- a temperature sensor circuit – the signals both from thermocouples and resistance sensors are transmitted into the buffer amplifier.

Buffering amplifiers are matched to each of the circuits, which is a unique solution, and they have the following characteristics:

- high input impedance not to burden the sensors connected,
- low output impedance to ensure sufficiently high current efficiency,
- high boundary frequency enables signals to be filtered.

5.5 Measurement system

Pressure sensors in a cylinder

Various measurement systems to measure working gas pressure are applied in research. The most frequent are piezoelectric quartz sensors that measure electric charges that arise when stress changes in quartz crystal due to pressure. These transducers are relatively expensive but they have very good properties. The example can be a Thermocomp 6061 quartz pressure sensor by Kistler (Figure 5.15). It is a water-cooled piezoelectric quartz sensor with an accuracy of a wide temperature range (-40 – 350 ºC) [77]. Its high sensitivity, i.e. 0.01%/ºC is due to the properties of quartz crystal and water cooling which keeps a sensor tip at a constant temperature. Cooling prevents from the thermal expansion of quartz crystal and membrane material. It is not only to protect the sensor from damage but also to maintain its measurement characteristics in a wide range of cylinder temperature.

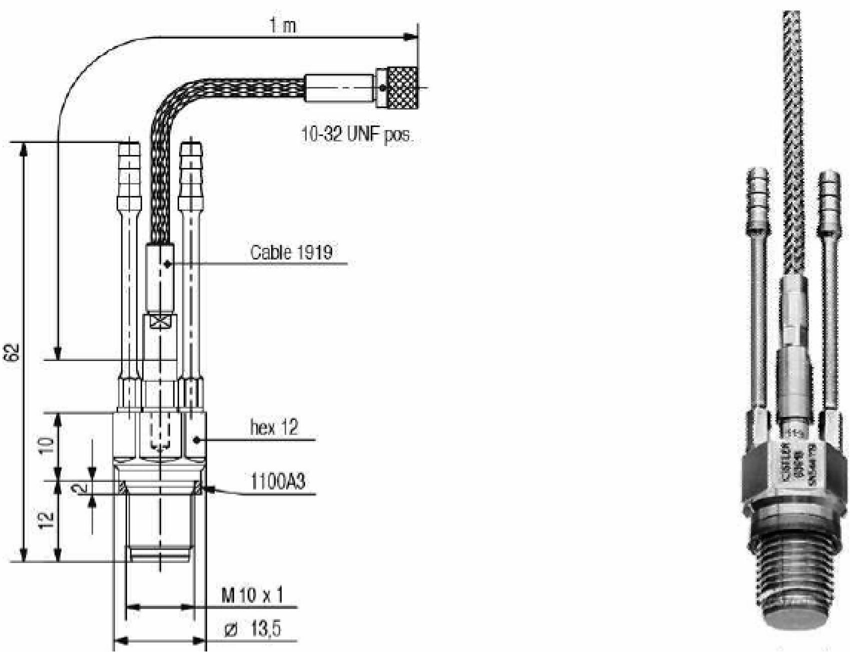

Fig. 5.15. Piezoelectric quartz sensors Kistler ThermoComp 6061 B [77]

By water cooling the sensor can be mounted directly in a combustion chamber. It is also possible to mount it with no cooling system. It is necessary then to place a detector far away from a combustion chamber and connect it using a thin channel. In diesel engines, it is possible to apply a sensor integrated with a glow plug.

An uncooled sensor that is mounted directly in a combustion chamber is a fiber optic pressure sensor by OPTRAND (Figure 5.16) [66]. The light emitted by an LED is reflected by a membrane surface. A photodiode registers the intensity of the light which changes depending on membrane deformation due to changes in pressure measured. The sensor measures the distance from the membrane surface. Light is delivered and taken back by optical fibers. An LED, photodiode and signal processing systems are located away from a cylinder head and equipment that emits electromagnetic radiation so that disturbances scarcely can influence this measurement, and a sensor part that is placed in a combustion chamber is small. The OPTRAND sensors integrated with a glow plug are also available [65].

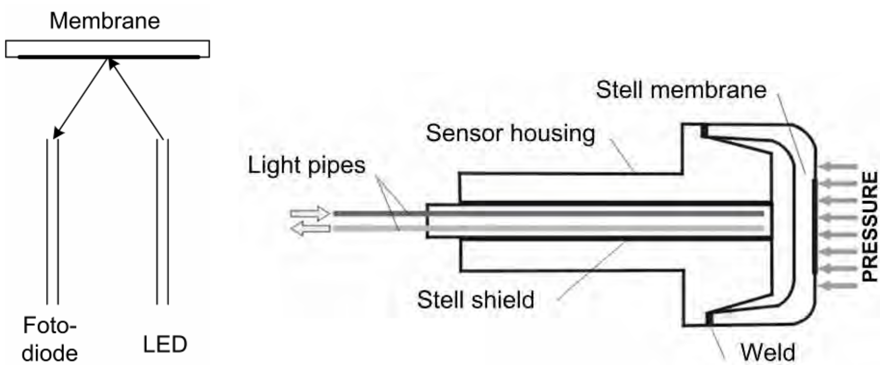

Fig. 5.16. Optic-fiber sensor OPTRAND – its operating principle and construction [66]

Many manufacturers and researchers try to construct a precise, disturbance-proof and reliable pressure sensor, e.g. piezoresistive glow plug sensors from BERU (Figure 5.17). They are mounted as standard in Audi Q7 automotive engines. A sensor membrane is far away from a combustion chamber [18], [25]. Pressure is transmitted onto this membrane through a movable heating element of a plug. Sensors by Denso that are integrated with a glow plug [57] or a spark plug [69] work in a similar way. Bosch patented a pressure cylinder sensor embedded in a piezoelectric injector with direct gasoline injection [49]. Kortez et al. [27] designed a silicon carbide pressure sensor. It was noted that it can be mounted in a combustion chamber due to its low sensitivity to temperature. Wendeker et al. [62] investigated an optical fiber cylinder pressure sensor. It was based on fiber deformation due to pressure changes. Wave interference was used to measure pressure.

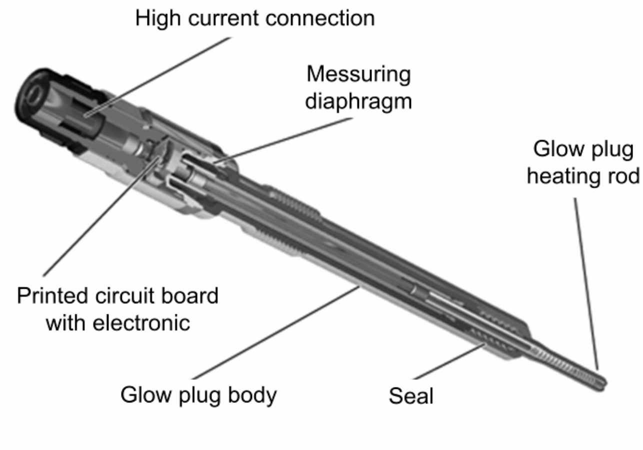

Fig. 5.17. Piezoresistive sensor by BERU [74]

Measurement systems

The research engine was equipped with additional sensors for monitoring engine performance. These were four MPX4250 pressure transducers under the throttle and two ones in each of the compressor inlet pipes and the head (Figure 5.18).

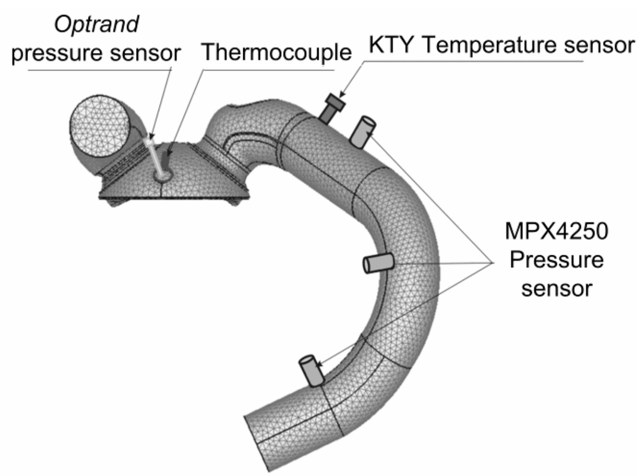

Fig. 5.18. Arrangement of the sensors to measure charge parameters

The pressure in the fuel system was measured with the MPX5700 sensor. MPX sensors by Motorola measure pressure difference in relation to the vacuum that deforms a chip, which changes output voltage (Figure 5.19). Their characteristics are given in Table 5.4.

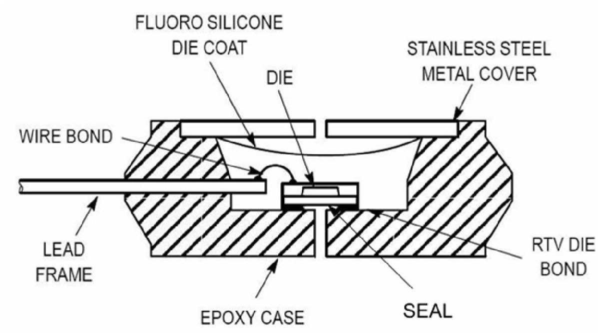

Fig. 5.19. Cross-sectional diagram of the MPX5700 sensor

Table 5.4. Characteristics of sensors MPX5700 and MPX4250

Quantity		**Min.**	**Type**	**Max.**	**Unit**
Destructive pressure		—	—	5000	kPa
Storage temperature		-40	—	125	°C
Operating temperature		-40	—	125	°C
Power input		—	7,0	10	mA
Response time		—	1,0	—	ms
Warm-up time		—	20	—	ms
MPX5700					
Pressure range		0	—	700	kPa
Permissible pressure		—	—	2800	kPa
Supply voltage		4,75	5,0	5,25	Vdc
Zero pressure offset	0 to 85 °C	0.088	0,2	0,313	Vdc
Full scale output	0 to 85 °C	4,587	4,7	4,813	Vdc
Full scale span	0 to 85 °C	—	4.5	—	Vd
Accuracy	0 to 85 °C	—	—	± 2,5	%VFSS
Sensitivity		—	6,4	—	mV/kPa
MPX5250					
Pressure range		0	—	250	kPa
Permissible pressure		—	—	1000	kPa
Supply voltage		4,85	5,1	5,35	Vdc
Zero pressure offset	0 to 85 °C	0,139	0,204	0,269	Vdc
Full scale output	0 to 85 °C	4,844	4,909	4,974	Vdc
Full scale span	0 to 85 °C	—	4,705	—	Vd
Accuracy	0 to 85 °C	—	—	± 1,4	%VFSS
Sensitivity		—	18,5	—	mV/kPa

Due to the number of cylinders in the engine tested, financial reasons influenced the choice of cylinder pressure sensors. Thus, optoelectronic pressure sensors M3.5x0.6 by Optrand were used to monitor the combustion process. They are quite cheap, and their technical parameters are sufficient for carrying out the said re-search. The sensors are in special adapters screwed in the engine heads.

The measurement system includes one LED and one photodiode. This system is permanently installed in the sensor so it can be miniaturized. Figure 5.20 shows the Optrand cylinder pressure sensors and its adapter that can be mounted in a combustion chamber. Their specifications and sensitivity are given Table 5.5 and 5.6, respectively.

Table 5.5. Technical specifications of the sensors by Optrand

Sensor symbol:	**M3.5x0.6**	**M4.5x0.5**
Quantities:	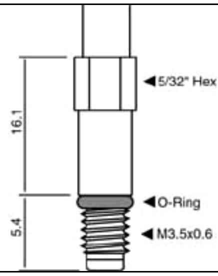	
Pressure range	0-0,1 MPa	
Cooling	no cooling is necessary	
Destructive pressure	2 x the measurement range or approx. 11,7 MPa	
Non-Linearity & Hysteresis (a full measurement range)	±0,5% of the measurement range (without combustion)	
	±1% of the measurement range (with combustion)	
Sensor output signal	analog, 0,5V to 5V	
Diagnostic output sensor	analog, 0V to 3,6V	
Diaphragm Resonant Frequency	≥120 kHz	
Frequency Range	0,01 Hz to 15 kHz	
n/s ratio	2000:1 (at 15kHz)	
Sensor Housing Temperature Range	-40 °÷300 °C (for continuous operation)	
Fibe-Optic Cable Operating Temperature	-40 °÷200 °C (for continuous operation)	
Fiber-Optic Cable Length	2 m (typical) or other (optionally)	
Fiber-Optic Cable Minimum	5 mm	

Bending Radius	
Signal Conditioner Operating Temperature Range	-20 °C to 125 °C
Temperature sensitivity coefficient	±0,003 %/°C
Pressure Media	gas or liquid
Output impedance	250 Ω
Voltage	9÷18 V
Supply voltage	50 mA (max. 85 mA)
Permissible acceleration	100 g
Guaranteed Lifetime	2 years in interrupted operation 3 years in continuous operation

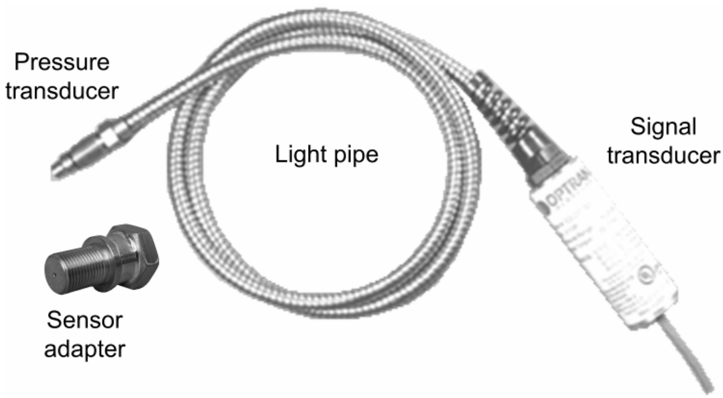

Fig. 5.20. Optoelectronic pressure sensors by Optrand and their adapter

Table 5.6. Sensitivity of the used pressure sensors by Optrand

Cylinder number	Sensor number	25 ˚C mV/MPa	200 ˚C mV/MPa
1	S/N6170B	435,1	422,1
2	S/N6168B	427,9	442,4
3	S/N6171B	433,7	433,7
4	S/N6152B	432,2	442,4
5	S/N6173B	417,7	422,1
6	S/N6172B	435,1	435,1
7	S/N6167B	433,7	427,9
8	S/N6150B	446,7	449,6
9	S/N6169B	467,0	446,7

The temperatures of the mixture and fuel in the fuel system were measured with KTY 19-6M/Z temperature sensors by Infineon (Figure 5.21). These are resistive sensors with a positive temperature coefficient. The characteristic of KTY sensors is shown in Table 5.7.

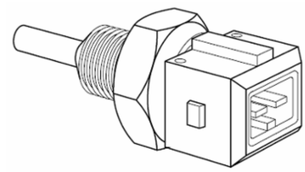

Fig. 5.21. Silicon temperature sensor KTY 19-6M/Z

Table 5.7. Characteristicc of sensor KTY 19-6M/Z

Quantity		**Value**	**Unit**
Maximum voltage	(25 ºC, 10 ms)	25	V
Maximum current		5	mA
Maximum momentary current	(25 ºC, 10 ms)	7	mA
Operation temperature		-50 - 150	°C
Resistance at 25°C		1980 - 2020	Ω
Assembling thread		M10 x 1	

The rotational speed and location of the crankshaft were measured with a specially designed adapter with two magnetoinductive sensors, 1GT101 Honeywell. The adapter was placed on the fuel pump shaft which rotates as fast as the crank-shaft. Its principle (Figure 5.22) is based on the switch that operates according to the Hall Effect and a magnet responsive to ferrous metals. This type of sensor has good properties at high (100 kHz) and low speeds. It is protected against reverse polarity and handles transients of up to +60/−40 V. The sensor has a digital open collector output. Its typical characteristics are given in Table 5.8.

Fig. 5.22. Magnetoinductive sensor Honeywell 1GT101

Table 5.8. Characteristics of the Honeywell magnetoinductive sensor

Quantity	Value	Unit
Supply voltage	+4,5 to +24	V
Supply current	10	mA
Output current	40	mA
Rise/fall time	15/1,0	ms max.
Temperature range	−40 to +150	°C

The amount of oxygen in exhaust gases is measured with the BOSCH LSU 4.2 wide-band lambda sensor (Table 5.9). An excess air ratio was registered with the LogWorks 2 software using the LM-1 digital meter by Innovate (Figure 5.23). In addition, the ratio is read from a digital indicator, but it is also possible to present its values as a text file. LogWorks 2 software enables the simultaneous measurement of several input signals (Figure 5.24).

Fig. 5.23. Gauge LM–1 and sensor BOSH LSU 4.2

Table 5.9. Technical specification of the BOSCH LSU 4.2 lambda sensor

Quantity	**Value**	**Unit**
Power supply	12	V
Exhaust gas temperature	930	ºC
Maximum exhaust gas temperature	1030	ºC
Heating time	30	s
Measuring range	0,5 – ∞	-
Reaction time	20	ms
Heating power	2	A
Linear range	0,5 – 3,5	-
Heater control frequency (max.)	2	Hz
Nominal resistance of Nernst cell	80	Ω

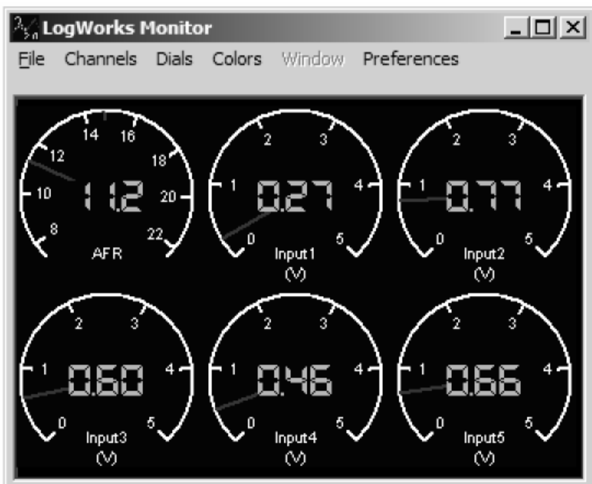

Fig. 5.24. User interface in LogWorks 2

In order to measure with the lambda sensor, the engine outlet system was modified. Single bent outlet pipes 250 mm long were mounted for stand tests. It is impossible to use lambda sensors in such pipes as the composition of exhaust gases and high temperature change. Under certain operation conditions, mixture finishes burning after it leaves an outlet system. The outlet system was modified by joining the outlet pipes of cylinder 3 and 4. Exhaust gas was not emitted directly into the atmosphere but decompressed in a tank of about 50 dm^3. The mixture composition can be averaged in such a tank. The last element of the system was a pipe 4 m long to prevent air to enter due to backflows.

5.6 Data processing system

The measurement data was collected using a National Instruments cDAQ-9172 measurement system with the NI 9215 measurement cards (Figure 5.25). These cards allow four analog signals ranging ± 10 V with a resolution of 16 bits and a maximum frequency of 100 kS/s to be measured simultaneously.

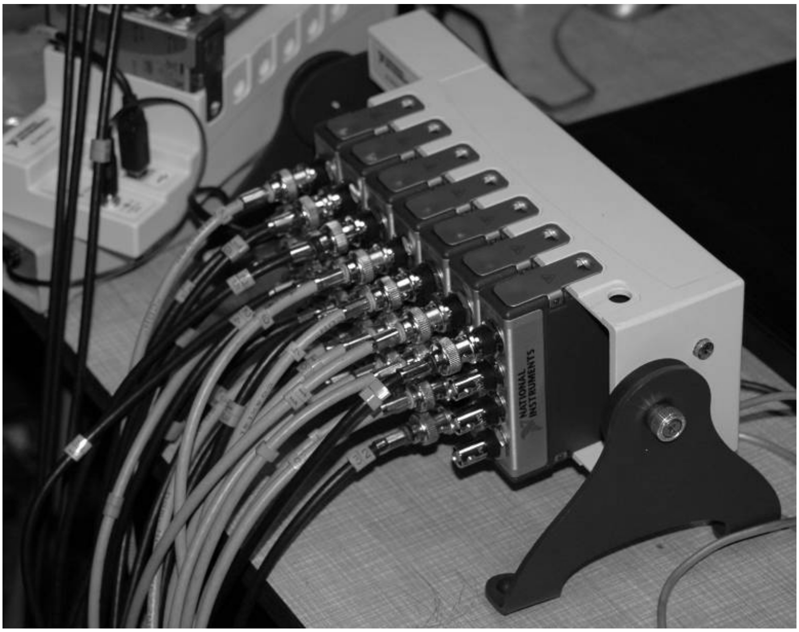

Fig. 5.25. Measurement system National Instruments cDAQ-9172

To record and pre-process the data, the two kinds of software were developed, i.e. to measure and analyze test result. Both of them were made using the LabVIEW 8.1.graphical programming environment.

Like Borland C or Borland Pascal, LabVIEW is ideal to develop your own software. The only difference is the way to create a software source code. In Lab-VIEW a source code is the graphically represented operations of the functions of entering (from a keyboard and devices), exiting (into a screen, printer and devices), information handling and processing and connections between the blocks; whereas in other environments, it is a sequential textual record in a particular programming language (Basic, C, Pascal). Recorded software in the G graphic language is as icons, clamps and connections to build virtually any gauge. LabVIEW software has extensive built-in libraries for data processing and sub-software for most programming tasks.

In Figure 5.26 is presented a software panel to record measurement data. The graphs show values measured. Figure 5.27 shows a part of a software code for data recording. Results of measurements are recorded as text files. The measurement was performed with a sampling rate of 100 000 samples per second.

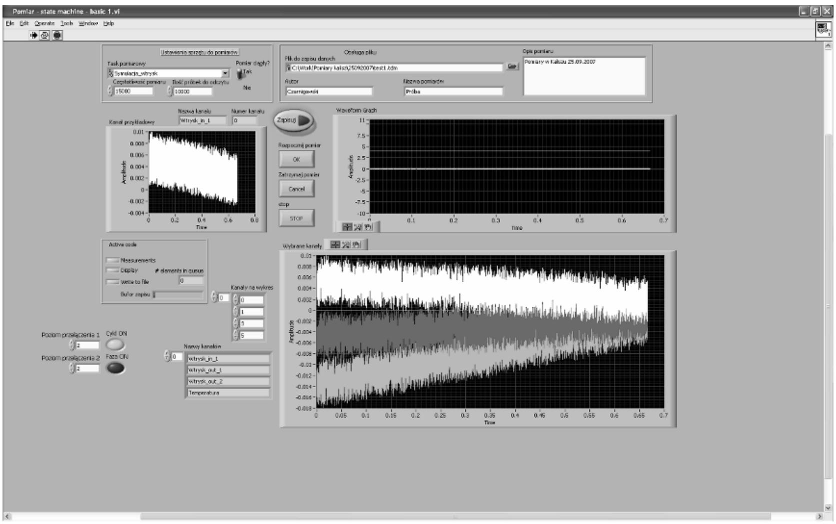

Fig. 5.26. Panel board for recording measurement data

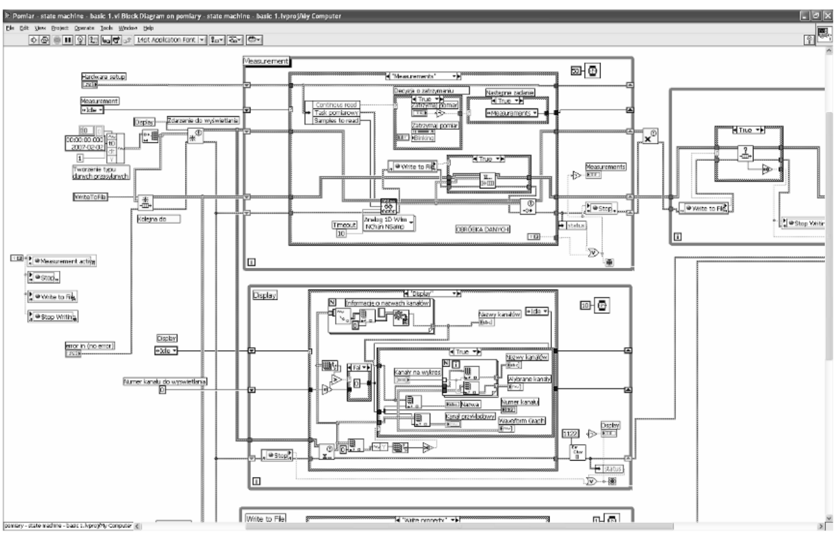

Fig. 5.27. Part of the programme code for data recording

The software for analysing test results (Figures 5.28 and 5.29) allows you to specify maximum cylinder pressure on the basis of measurement data recorded in text files.

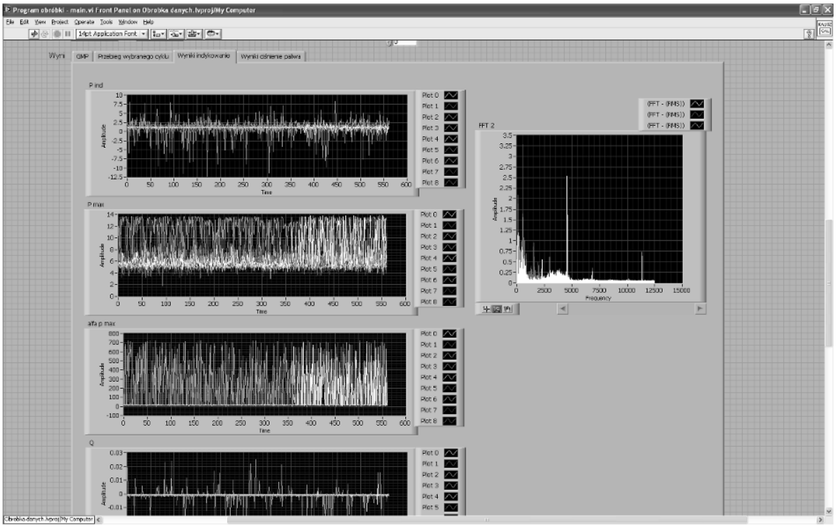

Fig. 5.28. Panel board for analyzing data obtained

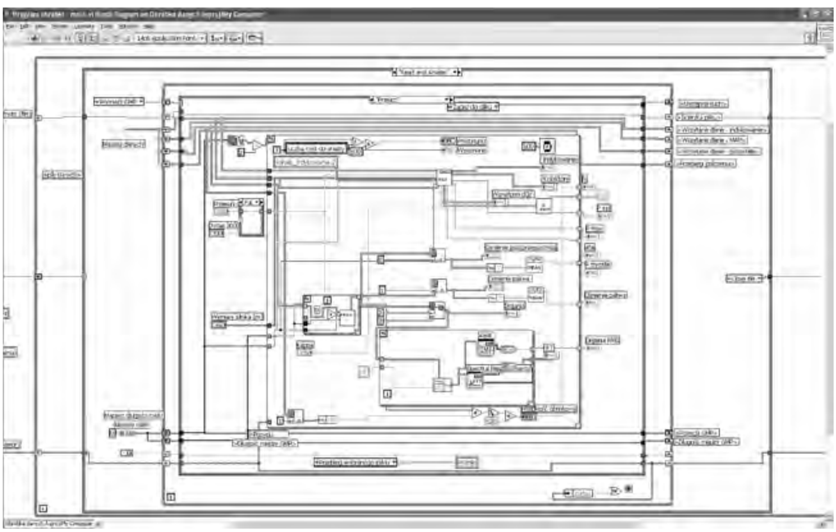

Fig. 5.29. Part of the programme code for data analyzing

To exchange data with the control unit of the engine, the Aviator software was developed (Figure 5.30). It is an application running under Windows on a PC. As a result, it is possible to read the indications of sensors mounted in the engine and to control the operation of fuel system components, i.e. switching on and off the fuel pump and controlling injector opening time. The software reads the following quantities:

- air excess ratio,
- crankshaft rotational speed,
- pressure in an intake pipe,
- fuel pressure,
- air temperature in an inlet pipe,
- engine head temperature,
- fuel temperature,
- up-to-date injection time.

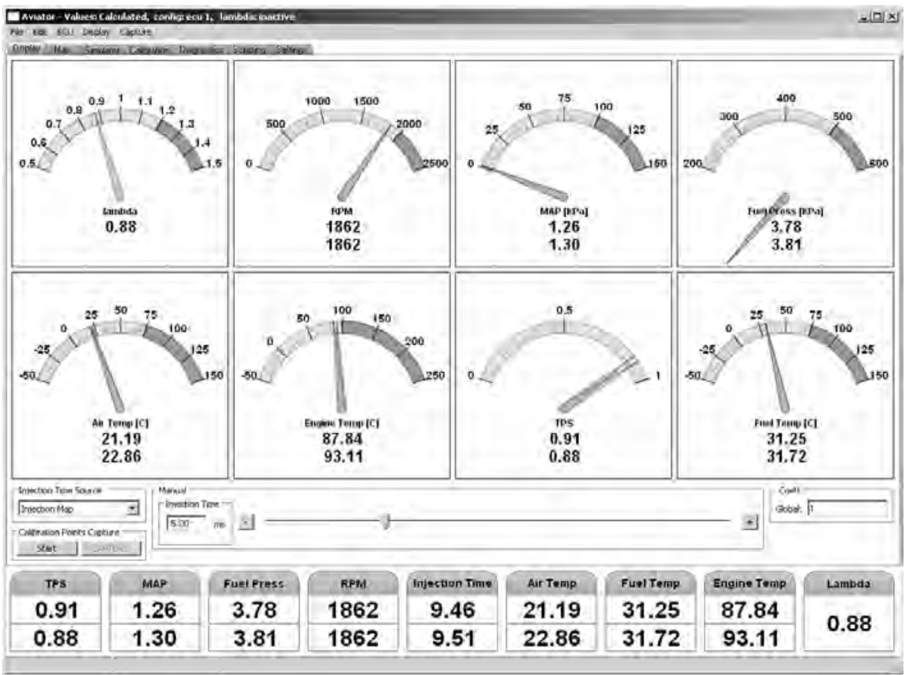

Fig. 5.30. Software panel board to communicate with the control unit

It is possible to record the changes of these quantities as a text file. The control software can also programme a control device. As soon as the control unit is programmed, it can work on its own (be disconnected from a PC). The control unit can control an engine in two ways:

a) it sets injector times depending only on rotational speed and load on the basis of characteristics recorded (Figure 5.31),
b) it calculates injection times using additionally correction algorithms recorded that use the indications of on-board sensors.

The control software can calibrate the indications of sensors. Calibration is necessary when the type of sensors used is changed. As a result, appropriate transducers can be selected. The software can diagnose the measurement and implementing elements of a fuel system and simulate engine operation. With the latter function, it is possible to verify the operation of a control unit without connecting it to an engine.

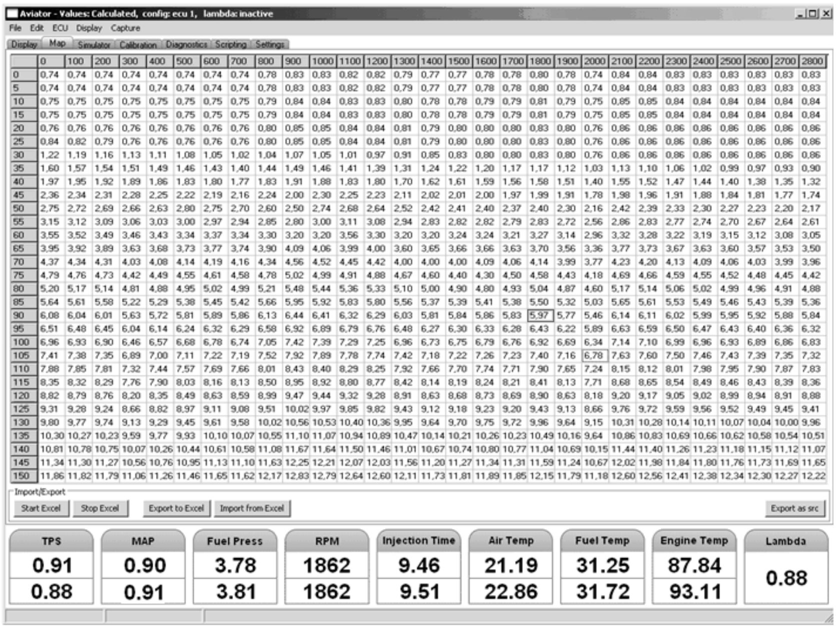

	0	100	200	300	400	500	600	700	800	900	1000	1100	1200	1300	1400	1500	1600	1700	1800	1900	2000	2100	2200	2300	2400	2500	2600	2700	2800
0	0,74	0,74	0,74	0,74	0,74	0,74	0,74	0,74	0,78	0,83	0,83	0,82	0,82	0,79	0,77	0,77	0,78	0,78	0,80	0,78	0,74	0,84	0,84	0,83	0,83	0,83	0,83	0,83	0,83
5	0,74	0,74	0,74	0,74	0,74	0,74	0,74	0,74	0,78	0,83	0,83	0,82	0,82	0,79	0,77	0,77	0,78	0,78	0,80	0,78	0,74	0,84	0,84	0,83	0,83	0,83	0,83	0,83	0,83
10	0,75	0,75	0,75	0,75	0,75	0,75	0,75	0,75	0,79	0,84	0,84	0,83	0,83	0,80	0,78	0,78	0,79	0,79	0,81	0,79	0,75	0,85	0,85	0,84	0,84	0,84	0,84	0,84	0,84
15	0,75	0,75	0,75	0,75	0,75	0,75	0,75	0,75	0,79	0,84	0,84	0,83	0,83	0,80	0,78	0,78	0,79	0,79	0,81	0,79	0,75	0,85	0,85	0,84	0,84	0,84	0,84	0,84	0,84
20	0,76	0,76	0,76	0,76	0,76	0,76	0,76	0,76	0,80	0,85	0,85	0,84	0,84	0,81	0,79	0,80	0,80	0,80	0,83	0,80	0,76	0,86	0,86	0,86	0,86	0,86	0,86	0,86	0,86
25	0,84	0,82	0,79	0,76	0,76	0,76	0,76	0,76	0,80	0,85	0,85	0,84	0,84	0,81	0,79	0,80	0,80	0,80	0,83	0,80	0,76	0,86	0,86	0,86	0,86	0,86	0,86	0,86	0,86
30	1,22	1,19	1,16	1,13	1,11	1,08	1,05	1,02	1,04	1,07	1,05	1,01	0,97	0,91	0,85	0,83	0,80	0,80	0,83	0,80	0,76	0,86	0,86	0,86	0,86	0,86	0,86	0,86	0,86
35	1,60	1,57	1,54	1,51	1,49	1,46	1,43	1,40	1,44	1,49	1,46	1,41	1,39	1,31	1,24	1,22	1,20	1,17	1,17	1,12	1,03	1,13	1,10	1,06	1,02	0,99	0,97	0,93	0,90
40	1,97	1,95	1,92	1,89	1,86	1,83	1,80	1,77	1,83	1,91	1,88	1,83	1,80	1,70	1,62	1,61	1,59	1,56	1,58	1,51	1,40	1,55	1,52	1,47	1,44	1,40	1,38	1,35	1,32
45	2,36	2,34	2,31	2,28	2,25	2,22	2,19	2,16	2,24	2,00	2,30	2,25	2,23	2,11	2,02	2,01	2,00	1,97	1,99	1,91	1,78	1,98	1,96	1,91	1,88	1,84	1,81	1,77	1,74
50	2,75	2,72	2,69	2,66	2,63	2,80	2,75	2,70	2,60	2,50	2,74	2,68	2,64	2,52	2,42	2,41	2,40	2,37	2,40	2,30	2,16	2,42	2,39	2,33	2,30	2,27	2,23	2,20	2,17
55	3,15	3,12	3,09	3,06	3,03	3,00	2,97	2,94	2,85	2,80	3,00	3,11	3,08	2,94	2,83	2,82	2,82	2,79	2,83	2,72	2,56	2,86	2,83	2,77	2,74	2,70	2,67	2,64	2,61
60	3,55	3,52	3,49	3,46	3,43	3,34	3,37	3,34	3,30	3,20	3,20	3,56	3,30	3,20	3,20	3,24	3,24	3,21	3,27	3,14	2,96	3,32	3,28	3,22	3,19	3,15	3,12	3,08	3,05
65	3,95	3,92	3,89	3,63	3,68	3,73	3,77	3,74	3,90	4,09	4,06	3,99	4,00	3,60	3,65	3,66	3,66	3,63	3,70	3,56	3,36	3,77	3,73	3,67	3,63	3,60	3,57	3,53	3,50
70	4,37	4,34	4,31	4,03	4,08	4,14	4,19	4,16	4,34	4,56	4,52	4,45	4,42	4,00	4,00	4,00	4,09	4,06	4,14	3,99	3,77	4,23	4,20	4,13	4,09	4,06	4,03	3,99	3,96
75	4,79	4,76	4,73	4,42	4,49	4,55	4,61	4,58	4,78	5,02	4,99	4,91	4,88	4,67	4,60	4,40	4,30	4,50	4,58	4,43	4,18	4,69	4,66	4,59	4,55	4,52	4,48	4,45	4,42
80	5,20	5,17	5,14	4,81	4,88	4,95	5,02	4,99	5,21	5,48	5,44	5,36	5,33	5,10	5,00	4,90	4,80	4,93	5,04	4,87	4,60	5,17	5,14	5,06	5,02	4,99	4,96	4,91	4,88
85	5,64	5,61	5,58	5,22	5,29	5,38	5,45	5,42	5,66	5,95	5,92	5,83	5,80	5,56	5,37	5,39	5,41	5,38	5,50	5,32	5,03	5,65	5,61	5,53	5,49	5,46	5,43	5,39	5,36
90	6,08	6,04	6,01	5,63	5,72	5,81	5,89	5,86	6,13	6,44	6,41	6,32	6,29	6,03	5,81	5,84	5,86	5,83	5,97	5,77	5,46	6,14	6,11	6,02	5,99	5,95	5,92	5,88	5,84
95	6,51	6,48	6,45	6,04	6,14	6,24	6,32	6,29	6,58	6,92	6,89	6,79	6,76	6,48	6,27	6,30	6,33	6,28	6,43	6,22	5,89	6,63	6,59	6,50	6,47	6,43	6,40	6,36	6,32
100	6,96	6,93	6,90	6,46	6,57	6,68	6,78	6,74	7,05	7,42	7,39	7,29	7,25	6,96	6,73	6,75	6,79	6,76	6,92	6,69	6,34	7,14	7,10	6,99	6,96	6,93	6,89	6,86	6,83
105	7,41	7,38	7,35	6,89	7,00	7,11	7,22	7,19	7,52	7,92	7,89	7,78	7,74	7,42	7,18	7,22	7,26	7,23	7,40	7,16	6,78	7,63	7,60	7,50	7,46	7,43	7,39	7,35	7,32
110	7,88	7,85	7,81	7,32	7,44	7,57	7,69	7,66	8,01	8,43	8,40	8,29	8,25	7,92	7,66	7,70	7,74	7,71	7,90	7,65	7,24	8,15	8,12	8,01	7,98	7,95	7,90	7,87	7,83
115	8,35	8,32	8,29	7,76	7,90	8,03	8,16	8,13	8,50	8,95	8,92	8,80	8,77	8,42	8,14	8,19	8,24	8,21	8,41	8,13	7,71	8,68	8,65	8,54	8,49	8,46	8,43	8,39	8,36
120	8,82	8,79	8,76	8,20	8,35	8,49	8,63	8,59	8,99	9,47	9,44	9,32	9,28	8,91	8,63	8,68	8,73	8,69	8,90	8,63	8,18	9,20	9,17	9,05	9,02	8,99	8,94	8,91	8,88
125	9,31	9,28	9,24	8,66	8,82	8,97	9,11	9,08	9,51	10,02	9,97	9,85	9,82	9,43	9,12	9,18	9,23	9,20	9,43	9,13	8,66	9,76	9,72	9,59	9,56	9,52	9,49	9,45	9,41
130	9,80	9,77	9,74	9,13	9,29	9,45	9,61	9,58	10,02	10,56	10,53	10,40	10,36	9,95	9,64	9,70	9,75	9,72	9,96	9,64	9,15	10,31	10,28	10,14	10,11	10,07	10,04	10,00	9,96
135	10,30	10,27	10,23	9,59	9,77	9,93	10,10	10,07	10,55	11,10	11,07	10,94	10,89	10,47	10,14	10,21	10,26	10,23	10,49	10,16	9,64	10,86	10,83	10,69	10,66	10,62	10,58	10,54	10,51
140	10,81	10,78	10,75	10,07	10,26	10,44	10,61	10,58	11,08	11,67	11,64	11,50	11,46	11,01	10,67	10,74	10,80	10,77	11,04	10,69	10,15	11,44	11,40	11,26	11,23	11,18	11,15	11,12	11,07
145	11,34	11,30	11,27	10,56	10,76	10,95	11,13	11,10	11,63	12,25	12,21	12,07	12,03	11,56	11,20	11,27	11,34	11,31	11,59	11,24	10,67	12,02	11,98	11,84	11,80	11,76	11,73	11,69	11,65
150	11,86	11,82	11,79	11,06	11,26	11,46	11,65	11,62	12,17	12,83	12,79	12,64	12,60	12,11	11,73	11,81	11,89	11,85	12,15	11,79	11,18	12,60	12,56	12,41	12,38	12,34	12,30	12,27	12,22

Fig. 5.31. Characteristic of injection time in relation to rotational speed and load

6. Results of the experiment

6.1 Introduction

This chapter describes the research objectives and plan of the experiment ac-cording to which the stand test was conducted. It also provides the results obtained from the experimental study.

6.2 Method of determining the parameters of a mixture formation model

The method is based on the time course of the maximum pressure in a cylinder p_{max} as a function of time during the jump-like changes in fuel dosing (Figure 6.1).

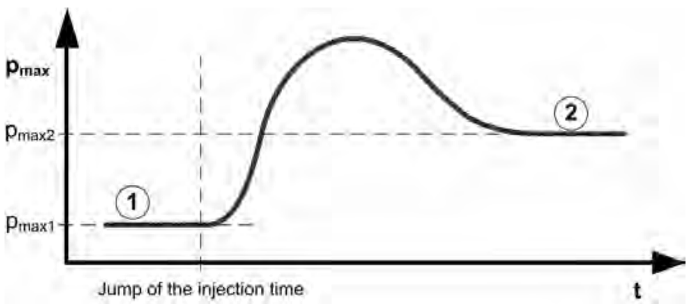

Fig. 6.1. Diagram of the time course of the maximum pressure in a cylinder p_{max} after a jump-like increase of a fuel dose

The initial value pmax1 and final p_{max2} of maximum pressure were marked on the characteristic of mass fuel in the cylinder (Figure 6.2). It should be noted that under steady-state conditions injection mass equals the fuel mass in a cylinder.

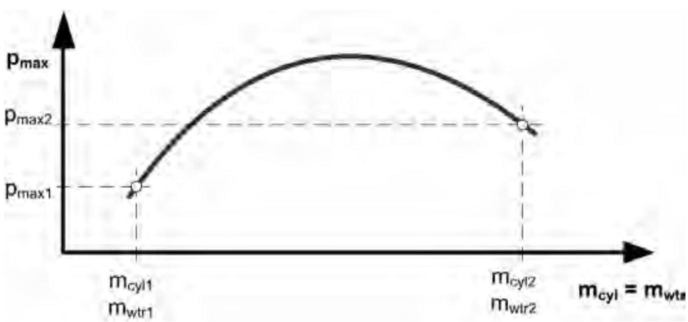

Fig. 6.2. Characteristics of the maximum pressure in a cylinder as a function of injected fuel mass

Knowing the above characteristic, the time course $p_{max}(t)$ can be replaced with that of $m_{cyl}(t)$ (Figure 6.3).

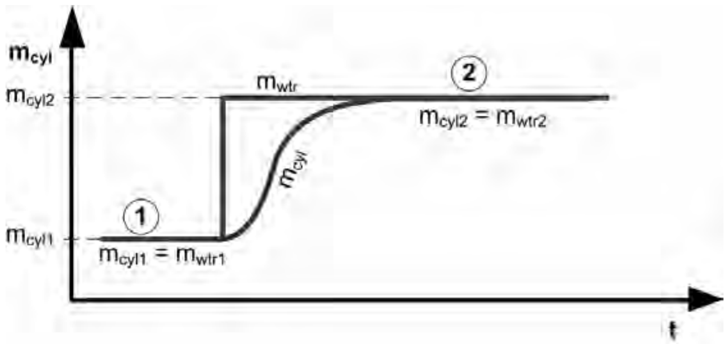

Fig. 6.3. Time course of the fuel mass in a cylinder m_{cyl} after a jump-like injection mass m_{wtr}

It was assumed that additional measurement points during jump-like injections are characterized by monotonic changes in fuel mass in a cylinder. A time moment t_{pmax} was determined as a starting point of one of the branches of the $p_{max}(m_{cyl})$ characteristic that was to determine fuel mass in a cylinder (Figure 6.4).

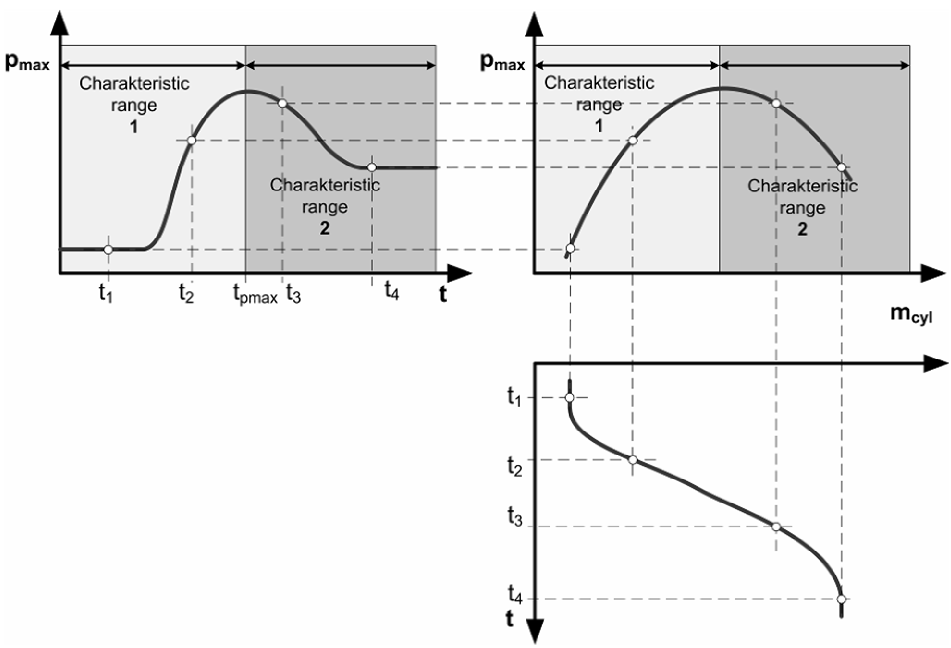

Fig. 6.4. Method of determining the time course of fuel mass in a cylinder m_{cyl}

The study to identify a model of mixture formation was two-stage. The first step was to make the characteristic of $p_{max}(m_{wtr})$. Given that injection mass depends linearly on injector opening time (Figure 6.5) (recorded during the research), the further analysis was based on injection time directly proportional to fuel mass.

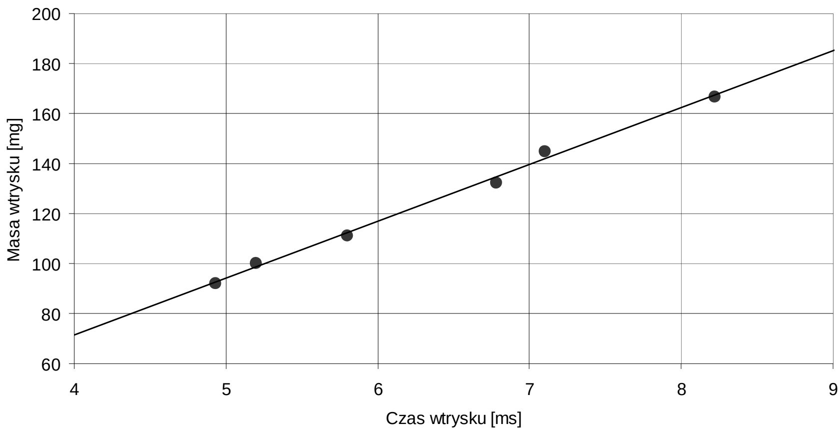

Fig. 6.5. Characteristic of the Bosch 0280150846 injector

Figure 6.4 is now as follows (Figure 6.6):

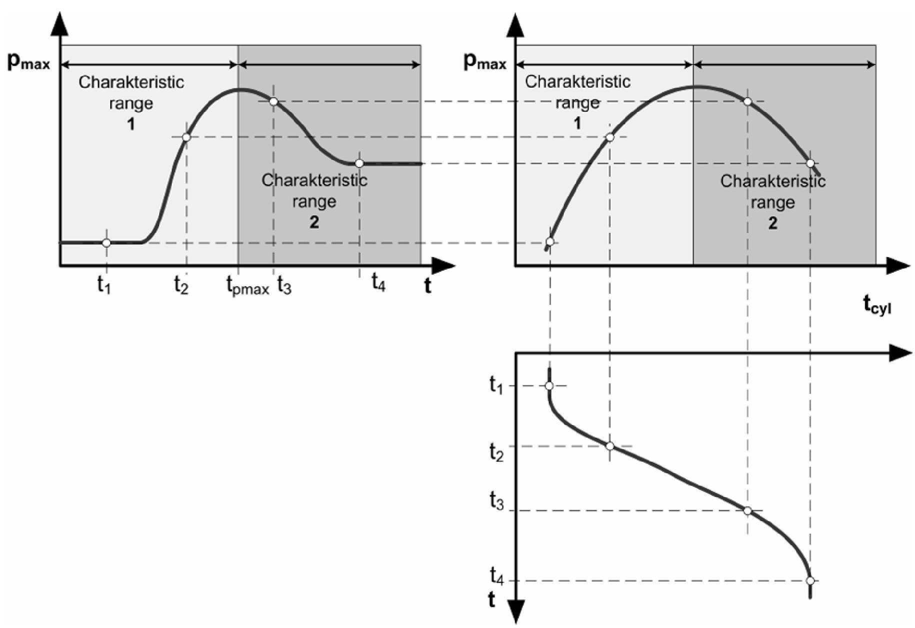

Fig. 6.6. Method of determining the time course of injection opening time t_{cyl} corresponding fuel mass in a cylinder m_{cyl}

6.3 Preliminary research

The preliminary research was conducted to determine the scope of identification research. It was done under steady operating conditions defined by:

- rotational speed 1770 rpm,
- charging pressure 94 kPa,
- oil temperature before the engine 60 ºC,
- oil temperature behind the engine 105 °C.

The values of pressure, temperature and speed correspond to working conditions rated at 60% of nominal power. These conditions stand for engine cruising speed. This is the most common working point under operation conditions. Fuel injection time was specified to obtain specific values of an excess air fuel ratio.

6.4 Analysis of the preliminary research

As a result of the preliminary tests, the characteristics of the relationship between an excess air ratio λ and injection time (Figure 6.7) and the time course of the maximum pressure in the cylinder depending on an excess air ratio (Figure 6.8) were done.

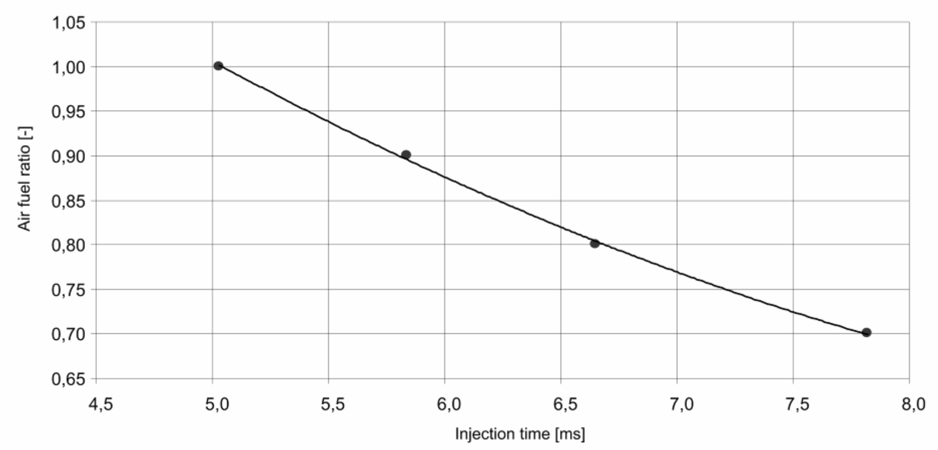

Fig. 6.7. Characteristic of the relationship between an excess air ratio and injection time

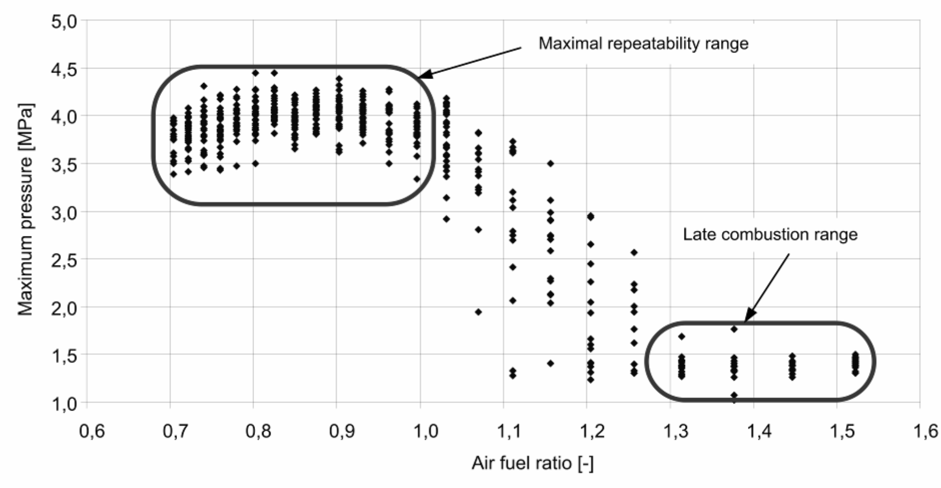

Fig. 6.8. Characteristic of the relationship between the cylinder maximum pressure and excess air ratio for cylinder 8

The analysis of the said results shows that the engine has the highest maximum pressure stability for mixture composition ranging from 0.7 to 1.0 and such a range of composition changes was adopted for testing in a transient state.

6.5 Schedule of the identification research

The two-stage identification tests included:

1. Research in a steady state.
2. Research in a transient state.

The studies in a steady state consisted of recording engine cylinder pressure during the gradual changes in injection time according to a particular sequence (Figure 6.9). To avoid hysteresis error when injection time was 7.6 ms (λ = 0.7), it was reduced again to 5.0 ms (λ = 1.0). During the testing eight cylinders worked with constant injection times, and the injection time of the 9th cylinder changed within 26 seconds from 5.0 ms to 7.6 ms. The injection time of the other cylinders was 5.84 ms, which corresponded to an excess air ratio λ = 0.9. This sequence was performed successively for all the cylinders.

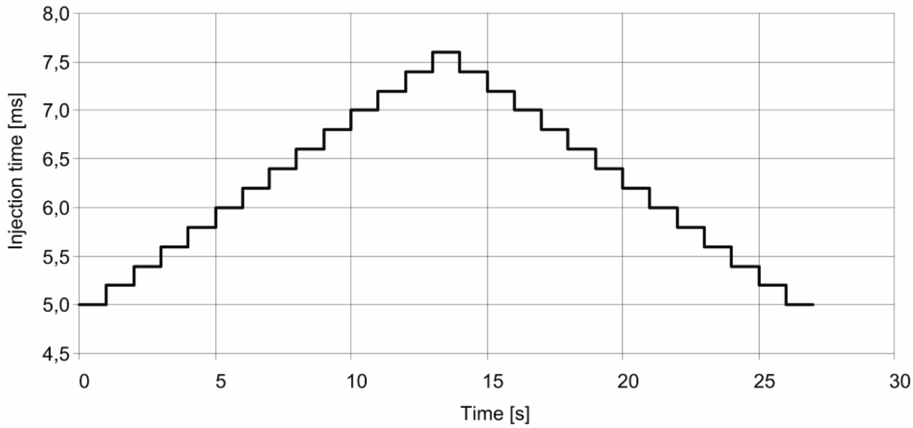

Fig. 6.9. Sequence of successive steady states while specifying the engine characteristic

The research under transient conditions included recording the cylinder pressure during a jump-like change of fuel injection time. The sequence of the changes in injection time is shown in Figure 6.10. To obtain more accurate measurements for each cylinder, injection time increased and decreased 6 times. Jump-like injection time changes ranged from 5.0 to 7.8 ms.

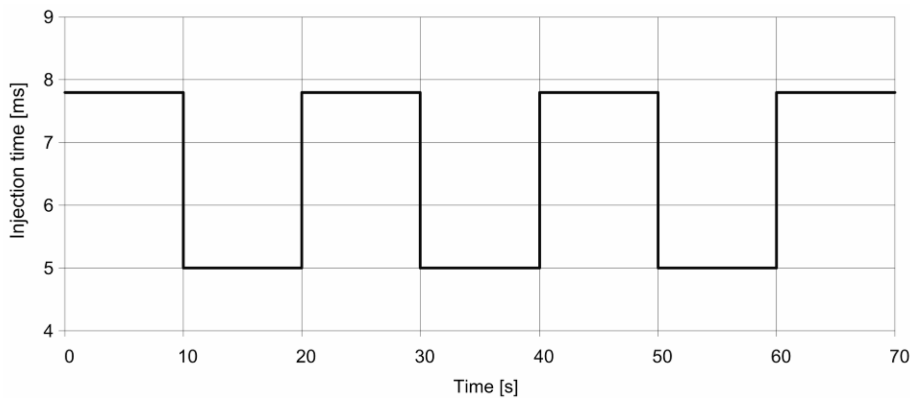

Fig. 6.10. Sequence of the changes in injection time in a transient state

6.6 Results of the identification research

The results of the experimental studies included the time courses of cylinder indicated pressure. These data were processed using LabVIEW to determine the value of the maximum cylinder pressure in successive cycles. Figure 6.11 shows an exemplary time course of the changes in maximum pressure obtained in a steady state. Figures from 6.12 to 6.20. shows the characteristic of the relationship between maximum pressure and injector opening time.

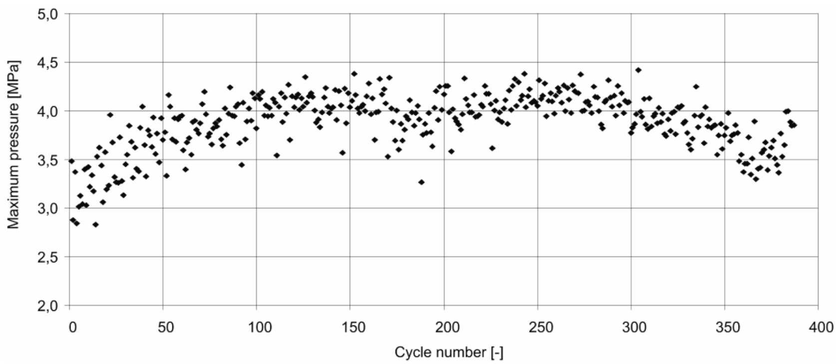

Fig. 6.11. Time course of the maximum pressure in cylinder 1 during the changes of injection time (in a quasi-steady state)

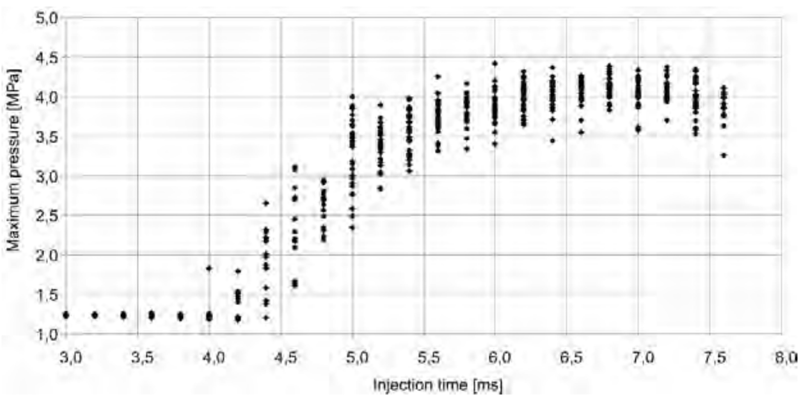

Fig. 6.12. Characteristics of the relationship between the cylinder maximum pressure and injector opening time for cylinder 1

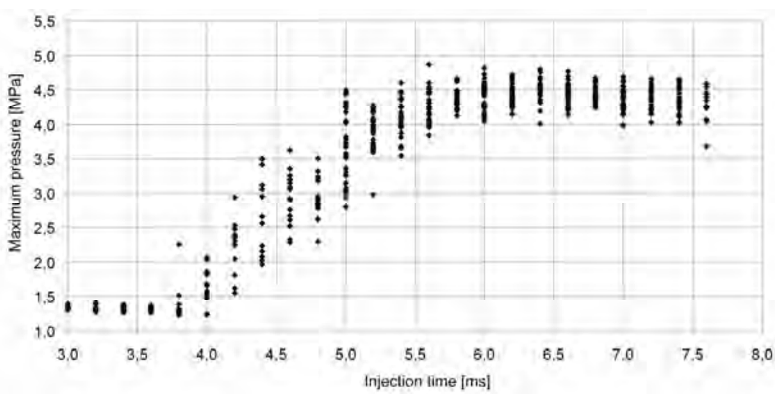

Fig. 6.13. Characteristics of the relationship between the cylinder maximum pressure and injector opening time for cylinder 2

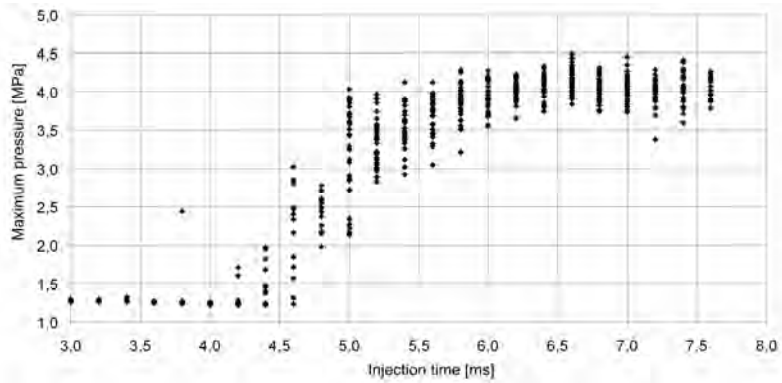

Fig. 6.14. Characteristics of the relationship between the cylinder maximum pressure and injector opening time for cylinder 3

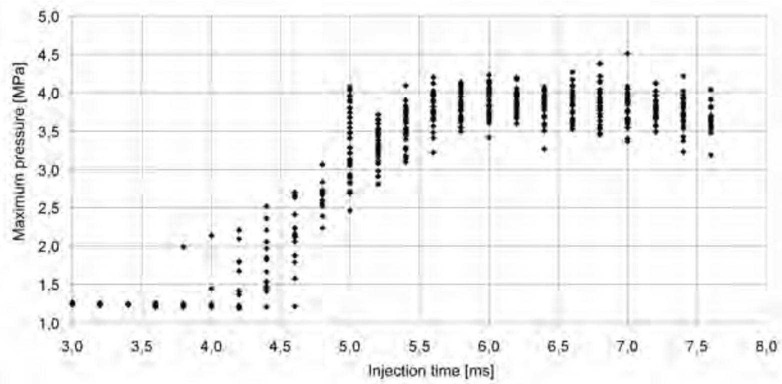

Fig. 6.15. Characteristics of the relationship between the cylinder maximum pressure and injector opening time for cylinder 4

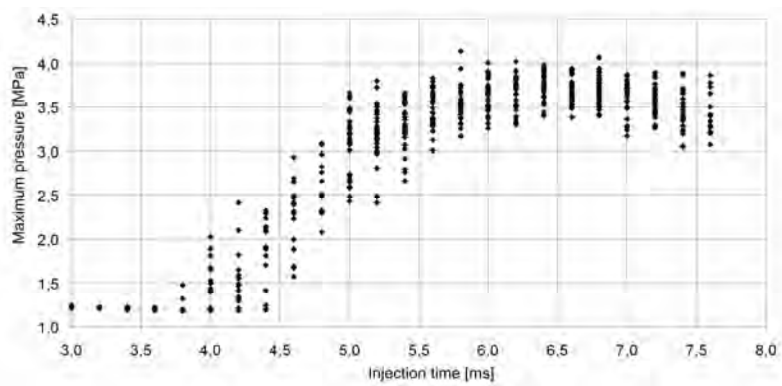

Fig. 6.16. Characteristics of the relationship between the cylinder maximum pressure and injector opening time for cylinder 5

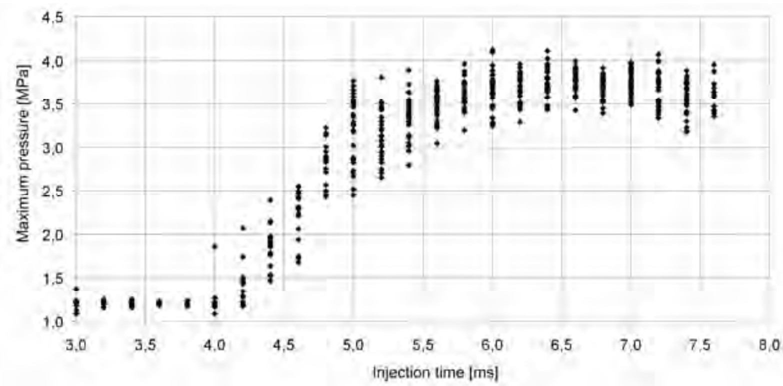

Fig. 6.17. Characteristics of the relationship between the cylinder maximum pressure and injector opening time for cylinder 6

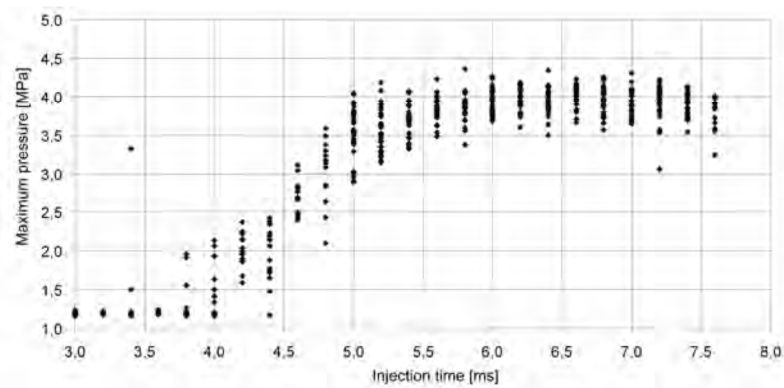

Fig. 6.18. Characteristics of the relationship between the cylinder maximum pressure and injector opening time for cylinder 7

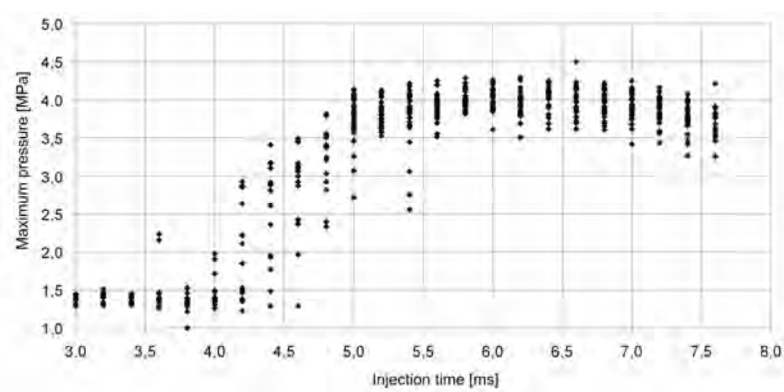

Fig. 6.19. Characteristics of the relationship between the cylinder maximum pressure and injector opening time for cylinder 8

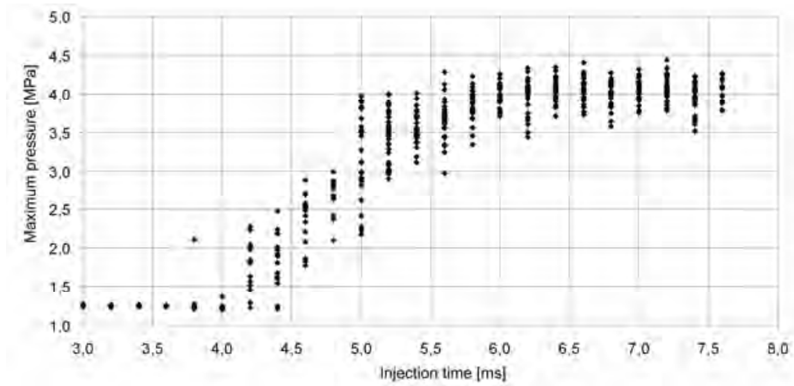

Fig. 6.20. Characteristics of the relationship between the cylinder maximum pressure and injector opening time for cylinder 9

The example of the results obtained in a transient state is given below. Figure 6.21 shows the time course of cylinder maximum pressure. The overlapping time courses from each jumps are shown in Figures from 6.22 to 6.39. The diagrams show the maximum pressure of 60 consecutive operation cycles. Injection time was changed in the 11th cycle.

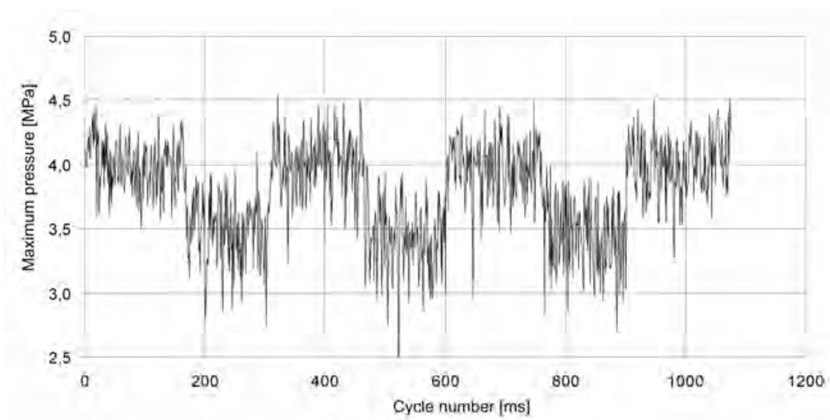

Fig. 6.21. Time course of the maximum pressure in cylinder 1 during the jumps of injection time

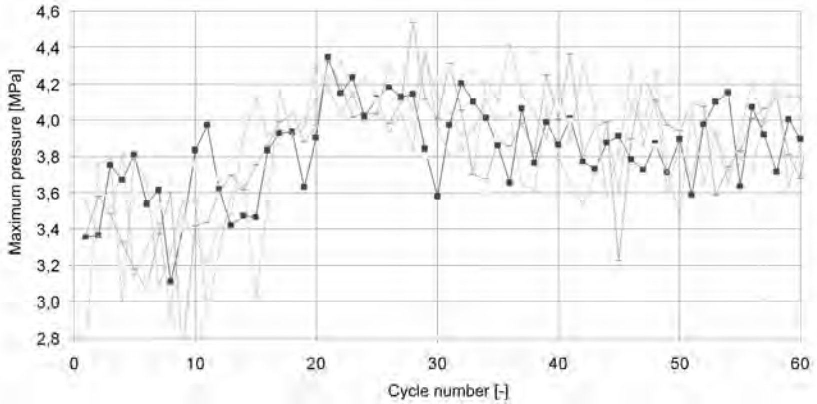

Fig. 6.22. Time course of the maximum pressure in cylinder 1 when injection time increased

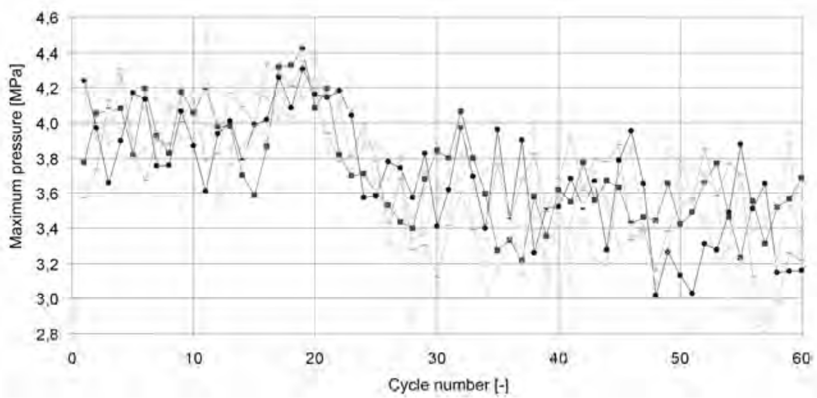

Fig. 6.23. Time course of the maximum pressure in cylinder 1 when injection time decreased

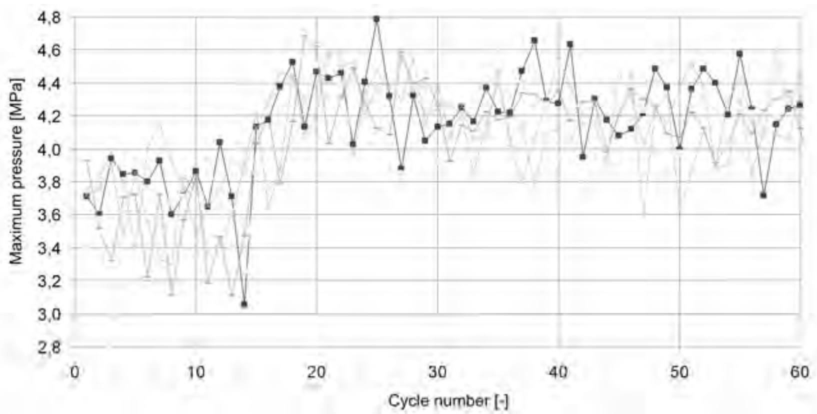

Fig. 6.24. Time course of the maximum pressure in cylinder 2 when injection time increased

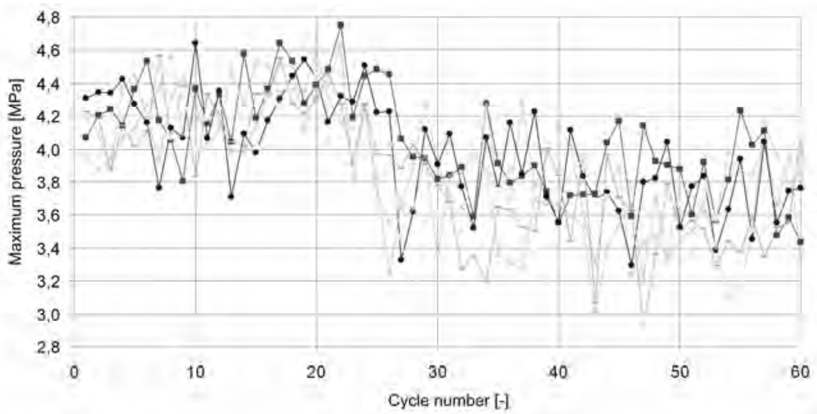

Fig. 6.25. Time course of the maximum pressure in cylinder 2 when injection time decreased

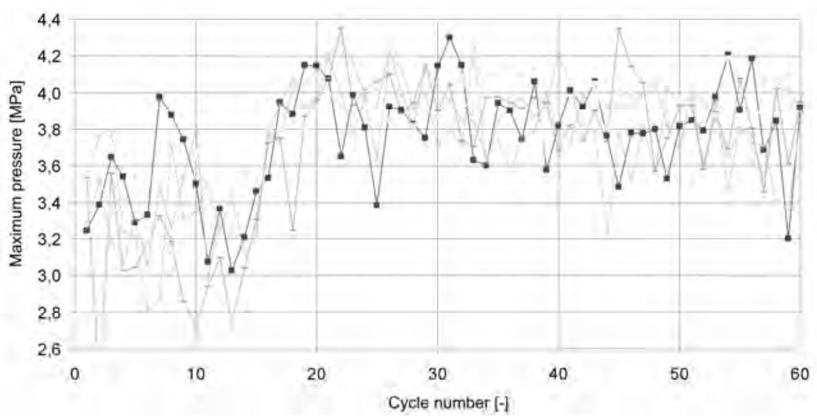

Fig. 6.26. Time course of the maximum pressure in cylinder 3 when injection time increased

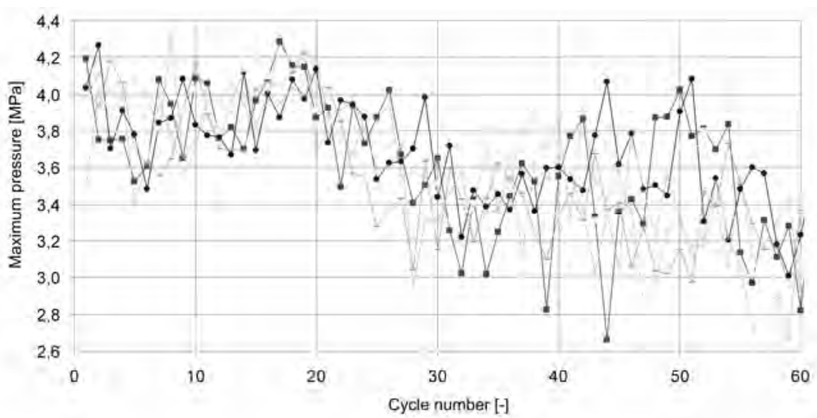

Fig. 6.27. Time course of the maximum pressure in cylinder 3 when injection time decreased

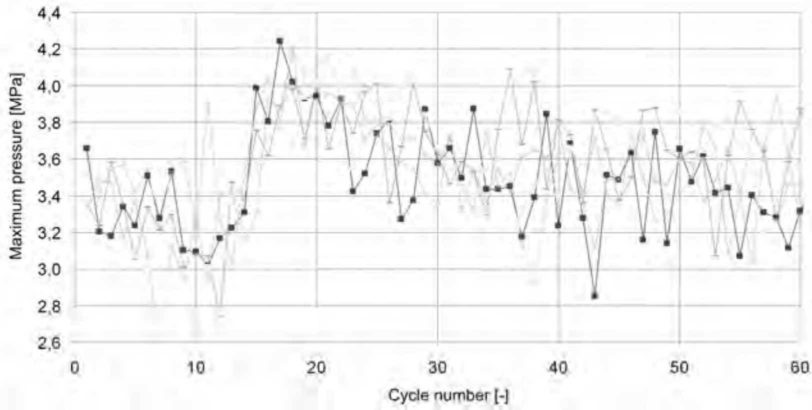

Fig. 6.28. Time course of the maximum pressure in cylinder 4 when injection time increased

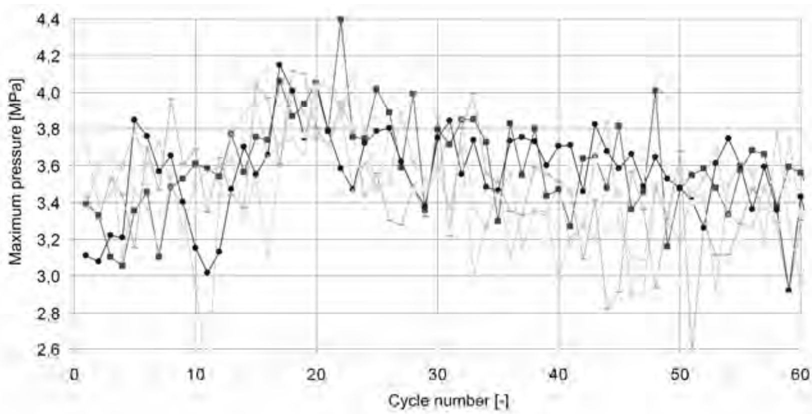

Fig. 6.29. Time course of the maximum pressure in cylinder 4 when injection time decreased

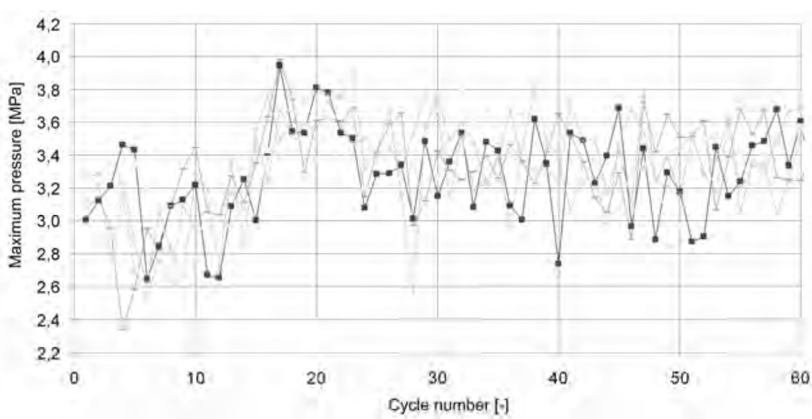

Fig. 6.30. Time course of the maximum pressure in cylinder 5 when injection time increased

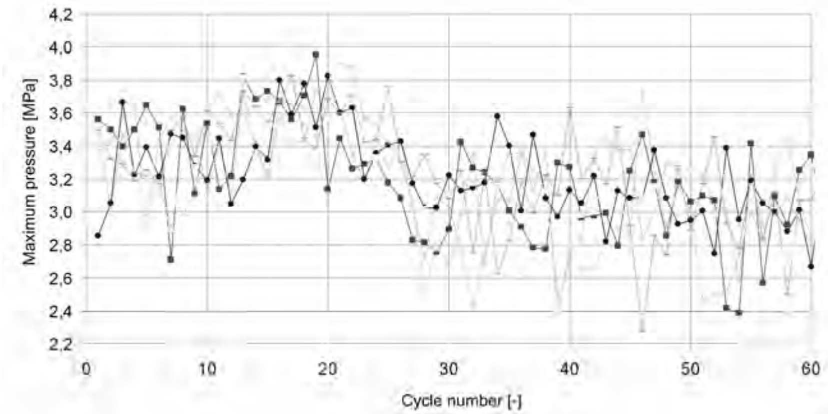

Fig. 6.31. Time course of the maximum pressure in cylinder 5 when injection time decreased

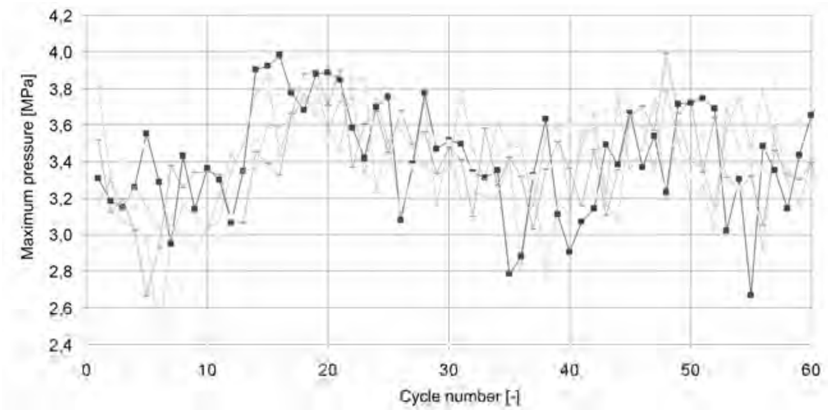

Fig. 6.32. Time course of the maximum pressure in cylinder 6 when injection time increased

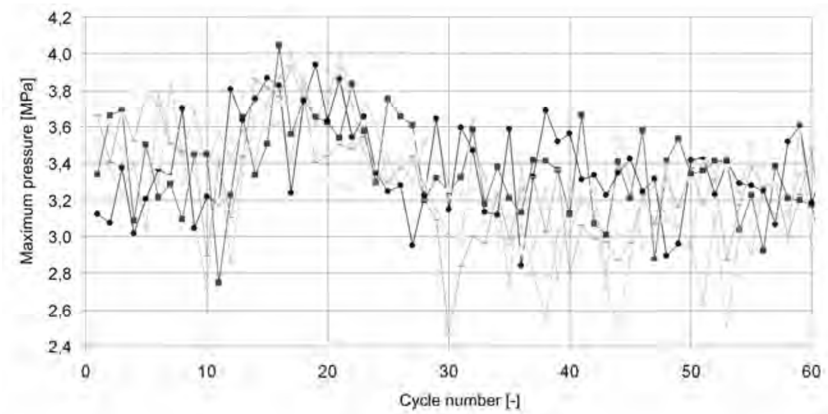

Fig. 6.33. Time course of the maximum pressure in cylinder 6 when injection time decreased

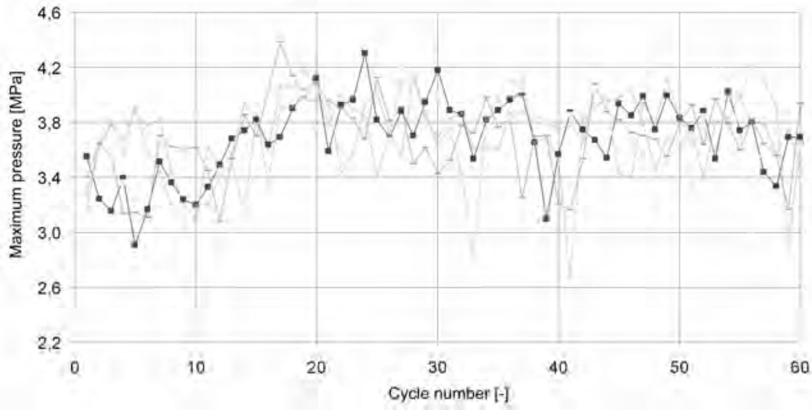

Fig. 6.34. Time course of the maximum pressure in cylinder 7 when injection time increased

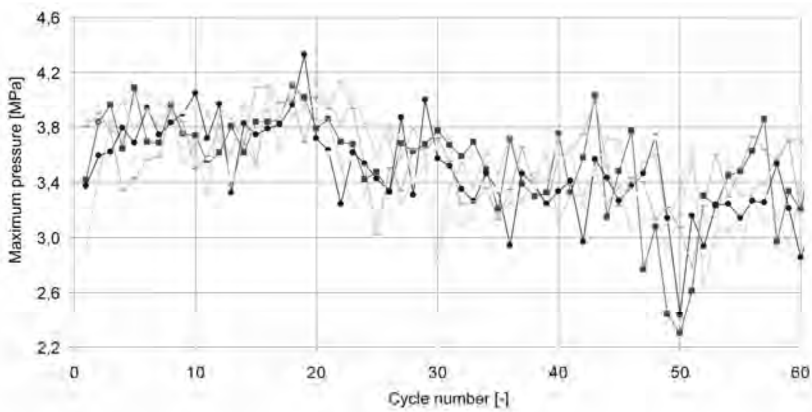

Fig. 6.35. Time course of the maximum pressure in cylinder 7 when injection time decreased

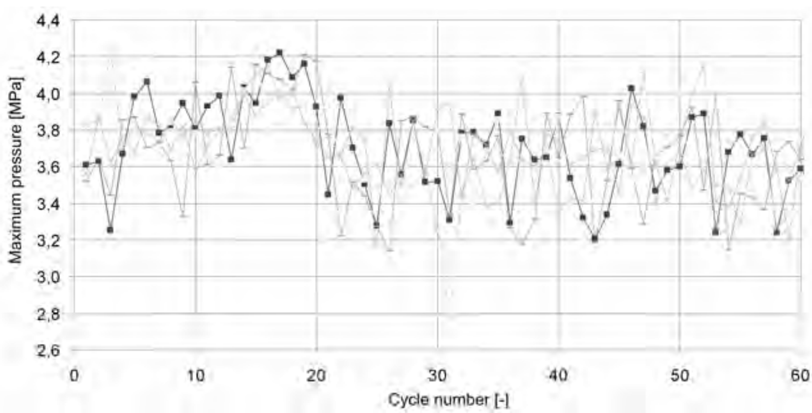

Fig. 6.36. Time course of the maximum pressure in cylinder 8 when injection time increased

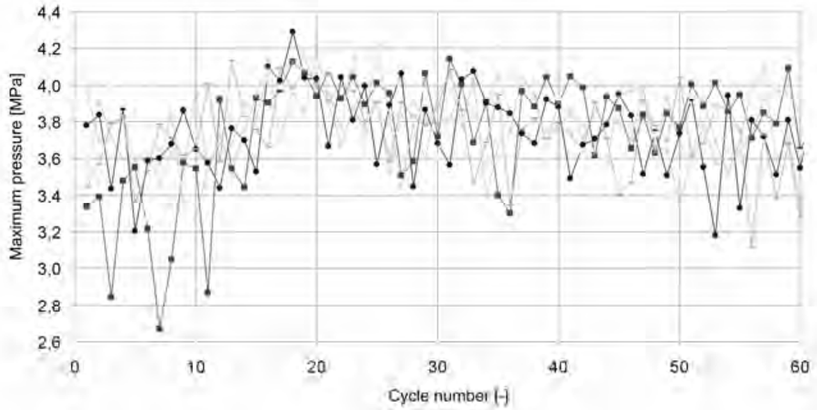

Fig. 6.37. Time course of the maximum pressure in cylinder 8 when injection time decreased

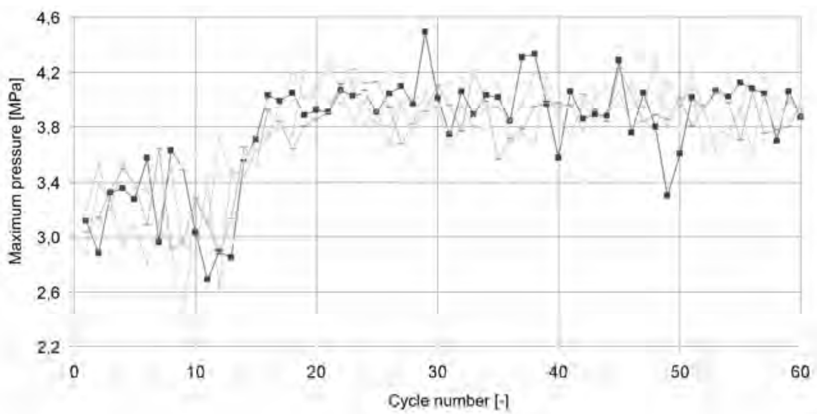

Fig. 6.38. Time course of the maximum pressure in cylinder 9 when injection time increased

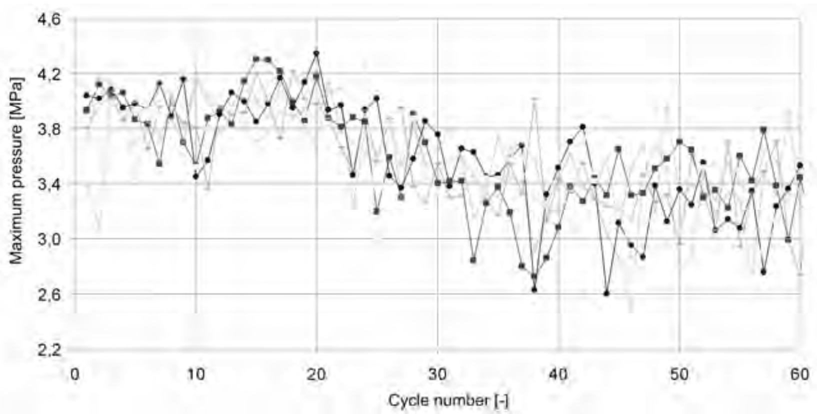

Fig. 6.39. Time course of the maximum pressure in cylinder 9 when injection time decreased

7. Analysis of the experiment results

7.1 Introduction

The chapter describes the procedure to identify the parameters of a fuel film model and the results and conclusions based on the analysis of the experimental results.

7.2 Identification procedure of a fuel film model

According to the procedure for analysing research results, there were obtained the time courses of injector opening time that stands for cylinder fuel mass (Figure 7.1).

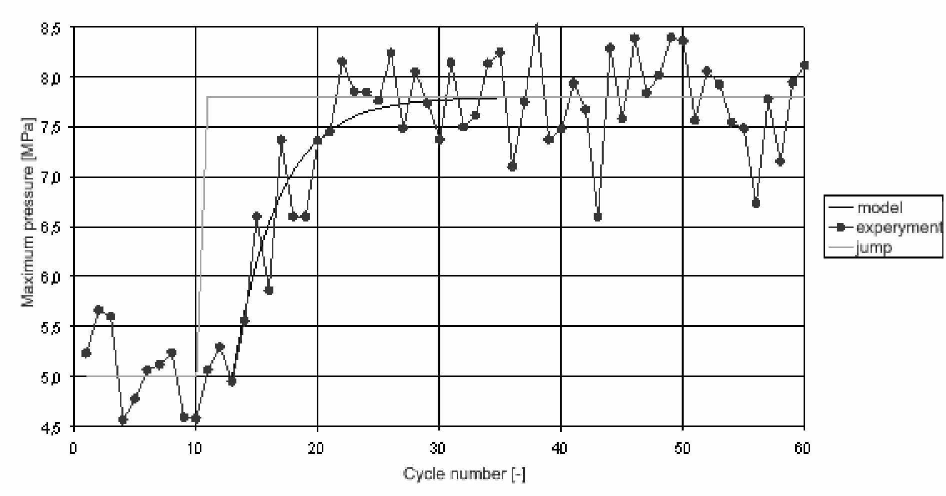

Fig. 7.1. Time course of the cylinder maximum pressure after a jupm of injection time – an example

Two issues can be noted while analysing the diagram in detail. First, it is clear that the entire fuel mass after injection settles on the walls. This is manifested by the slowly increasing maximum pressure after changing injection time. If this fuel percentage were less than 100, pressure would increase faster in the first cycles after the change, which is explained in Figure 7.2.

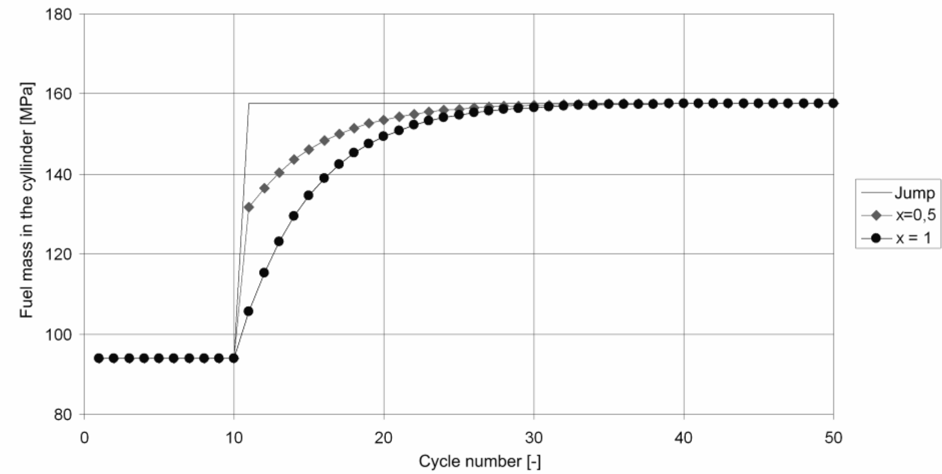

Fig. 7.2. Time course of the cylinder maximum pressure after a fuel dose jump for varied film coefficient x

Thus, the film coefficient after injection was assumed to be 1.0. The second observation is related to the proposition that there is a delay in transporting fuel in the intake pipe that consists in the "freezing" of the next injections on the walls of the intake pipe and a significant importance of the phenomenon of "pushing" fuel into cylinders by air pressure and gravity (Figure 7.3).

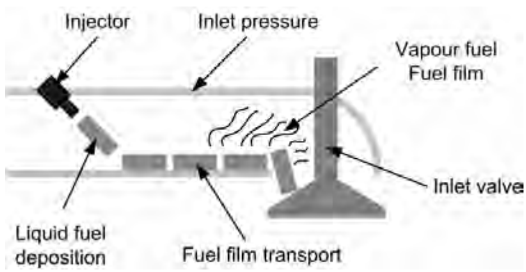

Fig. 7.3. Phenomena of fuel transportation from an injector to a cylinder

It is therefore a simplified model of fuelling a cylinder:

$$m_{cyl}(t) = \frac{m_{cyl}(t-\Delta t)\cdot\dfrac{\tau}{\Delta t} + m_{wtr}(t-\gamma\cdot\Delta t)}{\dfrac{\tau}{\Delta t}+1}, \qquad (7.1)$$

where:

Δt – time between successive cycles,

τ – film time-constant,

γ – number of engine cycles during transporting a non-evaporating fuel along the inlet pipe.

Under steady-state conditions:

$$m_{cyl}(t) = m_{wtr}(t - \gamma \cdot \Delta t)\,, \tag{7.2}$$

$$m_{cyl}(t) \cdot \left(\frac{\tau}{\Delta t} + 1 \right) = m_{cyl}(t) \cdot \frac{\tau}{\Delta t} + m_{wtr}(t)\,, \tag{7.3}$$

which means that:

$$m_{cyl}(t) = m_{wtr}(t)\,. \tag{7.4}$$

The parametric identification of the model means specifying the values of τ and γ. The equation in (7.1) is as follows:

$$\hat{t}_{cyl}(i) = \frac{\hat{t}_{cyl}(i-1) \cdot \frac{\tau}{\Delta t} + t_{wtr}(i-\gamma)}{\frac{\tau}{\Delta t} + 1}\,, \tag{7.4}$$

where:

i – successive-cycle index,

$t = i \cdot \Delta t$,

t_{wtr} – set injector opening time,

t_{cyl} – modelled injector opening time proportional to the fuel mass in a cylinder.

Under steady-state conditions:

$$\hat{t}_{cyl}(i) = \hat{t}_{cyl}(i-1) = t_{wtr}(i)\,. \tag{7.5}$$

The method of least squares was to calculate τ and cylinder. Thus, an S functional was used:

$$S = \sum_{i=i_1}^{i=i_2} \left[\hat{t}_{cyl}(i) - t^{*}{}_{cyl}(i) \right]^2\,, \tag{7.6}$$

where:

$t^{*}{}_{cyl}(i)$ - injection time obtained in i-time cycle,

$\hat{t}_{cyl}(i)$ - injection time calculated in a model for the set values of τ and γ,

i_1, i_2 – initial and final number of the tested injection in a transient state.

Arbitrarily, it was assumed that i1 = 11 (jump start) and i2 = 31 (first 20 cycles after a jump). A minimum identification error or the minimum of an S functional can be obtained for an optimal pair (τ, γ), which is usually formulated as:

$$S \to \min \equiv \frac{\partial S}{\partial \gamma} = 0\,,\ \frac{\partial S}{\partial \tau} = 0\,. \tag{7.7}$$

To determine an optimal pair (τ, γ) that ensures a minimum modeling error, the method for searching space $\tau \in$ {0, 1000 ms}, $\tau \in$ {0, 6} with an accuracy of $\Delta\tau$ = 10 ms, $\Delta\gamma$ = 1. The optimal values of $\gamma_{n,\,m\,,s}$, $\tau_{n,\,m,\,s}$ were determined for each of the 6 pairs of consecutive strokes for each cylinder, where:

n - number of a successive cylinder (*n* = 1 ... 9),
m - number of a successive stroke (*m* = 1 ... 6),
s - number of a jump type: *s* = 0 (drop), *s* = 1 (fuel dose increase).

Then, the average values for the next cylinders were calculated (separately for a drop and fuel dose increase):

$$\bar{\gamma}_{n,s} = \frac{\sum_{m=1}^{6} \gamma_{m,n,s}}{m}, \tag{7.8}$$

$$\bar{\tau}_{n,s} = \frac{\sum_{m=1}^{6} \gamma_{m,n,s}}{m}. \tag{7.9}$$

The subsequent calculations were to determine standard deviations ∂_γ and ∂_τ that were used later for statistical tests.

7.3 Results of the identification research

Approximating the relationship of the maximum pressure in the cylinder and injector opening time was done first in the identification testing. Figures from 7.4 to 7.12 show approximation results for each cylinders.

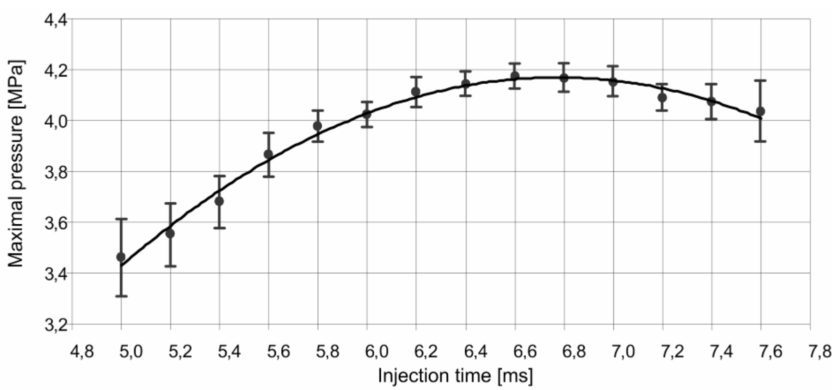

Fig. 7.4. Relationship between the maximum cylinder pressure and injector opening time for cylinder 1 and the approximation by an exponential curve

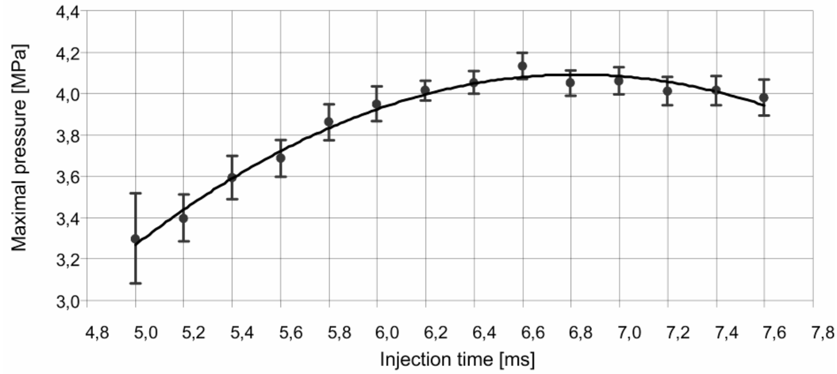

Fig. 7.5. Relationship between the maximum cylinder pressure and injector opening time for cylinder 2 and the approximation by an exponential curve

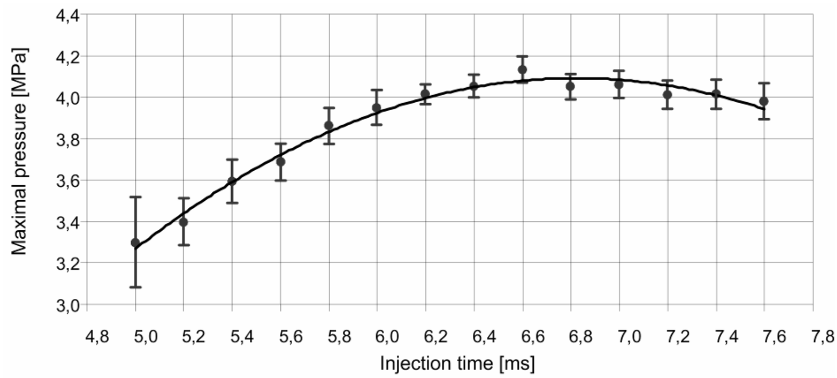

Fig. 7.6. Relationship between the maximum cylinder pressure and injector opening time for cylinder 3 and the approximation by an exponential curve

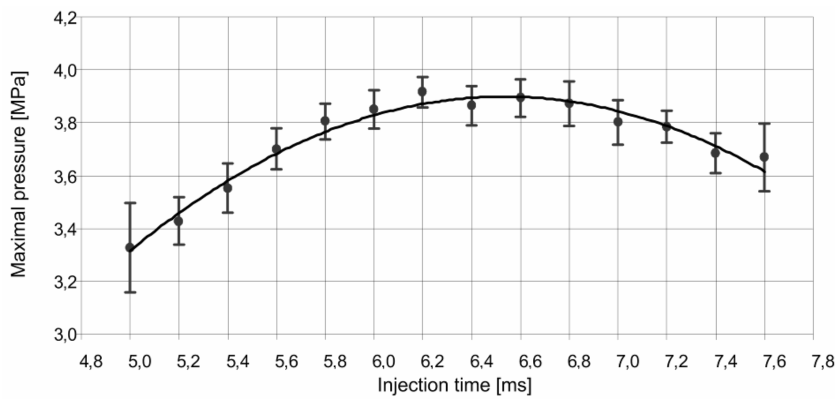

Fig. 7.7. Relationship between the maximum cylinder pressure and injector opening time for cylinder 4 and the approximation by an exponential curve

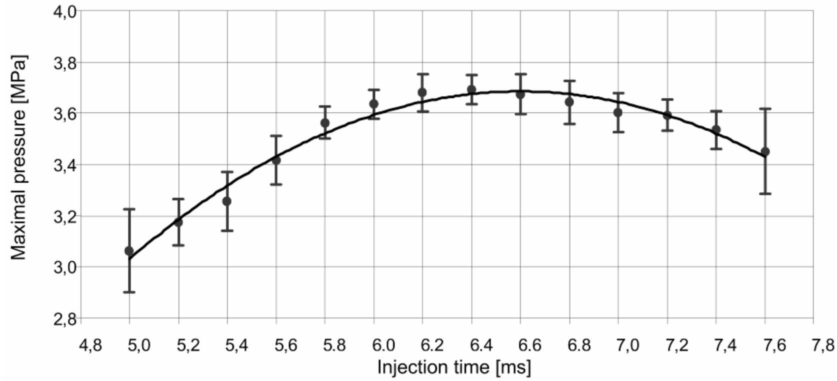

Fig. 7.8. Relationship between the maximum cylinder pressure and injector opening time for cylinder 5 and the approximation by an exponential curve

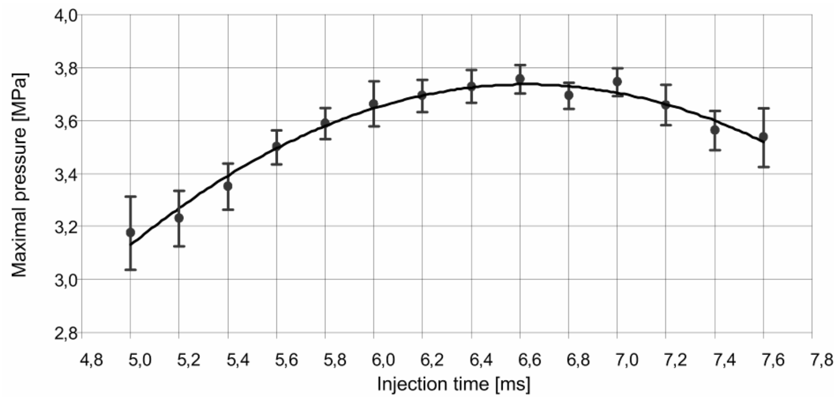

Fig. 7.9. Relationship between the maximum cylinder pressure and injector opening time for cylinder 6 and the approximation by an exponential curve

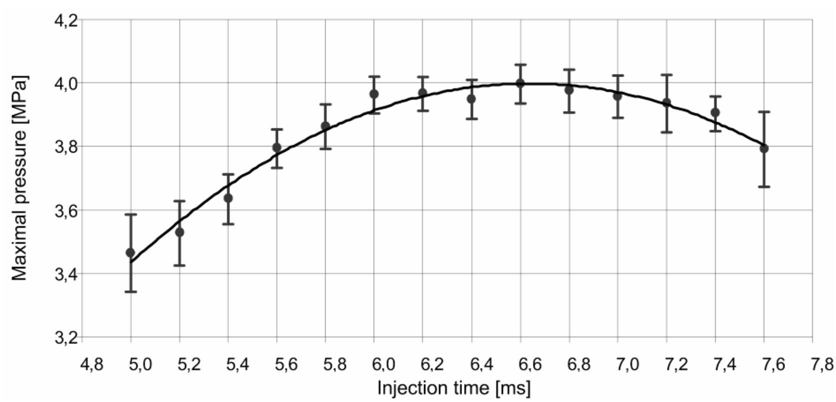

Fig. 7.10. Relationship between the maximum cylinder pressure and injector opening time for cylinder 7 and the approximation by an exponential curve

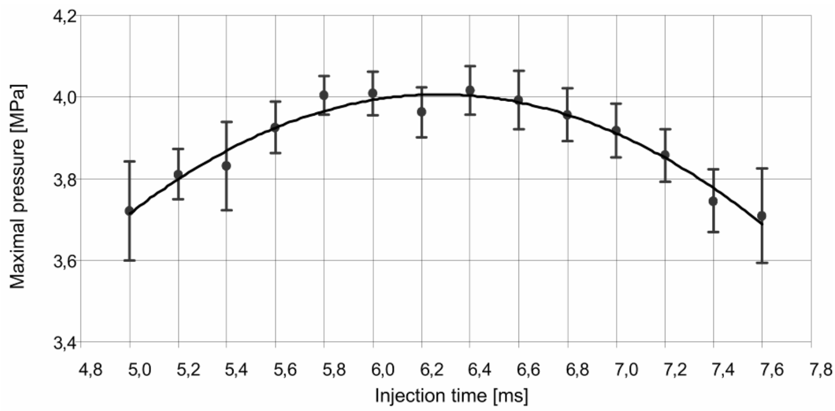

Fig. 7.11. Relationship between the maximum cylinder pressure and injector opening time for cylinder 8 and the approximation by an exponential curve

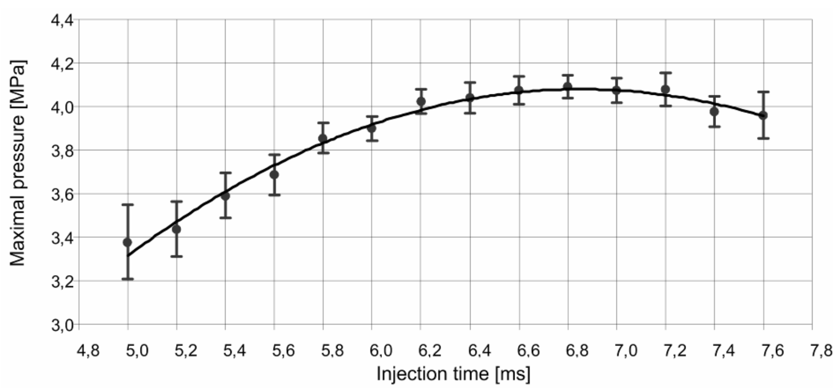

Fig. 7.12. Relationship between the maximum cylinder pressure and injector opening time for cylinder 9 and the approximation by an exponential curve

The results of identification calculations of parameters for model γ and τ are shown in radar charts (Figures 7.13 and 7.14). They show average values of the decreases and increases in the injection time and average values for both types of jumps.

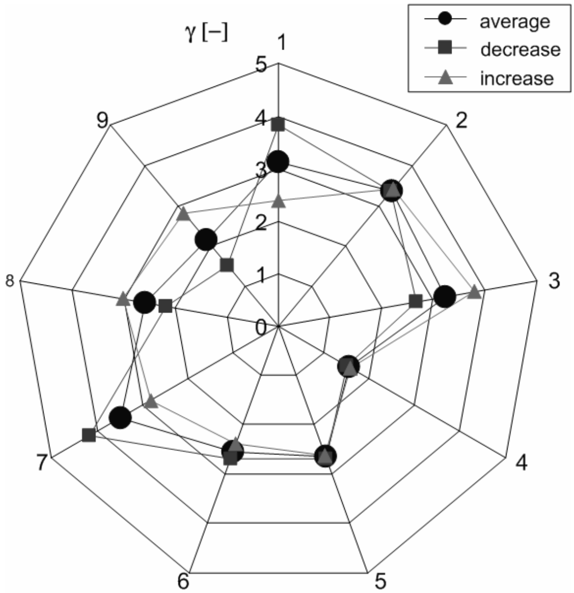

Fig. 7.13. Distribution of the mean vales of parameter *γ* for individual cylinders

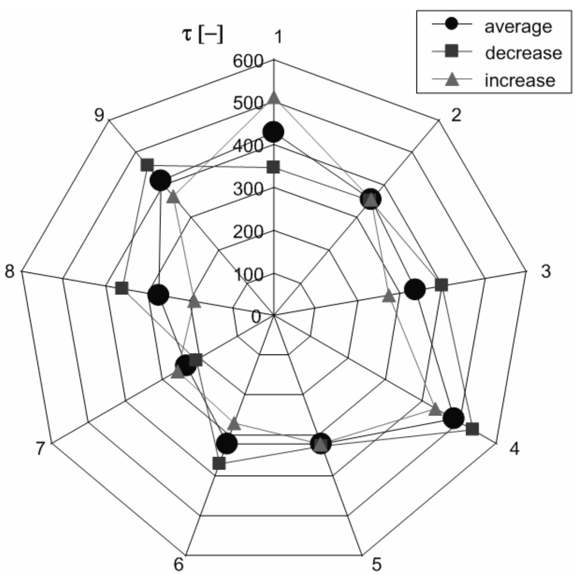

Fig. 7.14. Distribution of the average values of parameter *τ* for individual cylinders

The coefficient Lc(99) was adopted to compare directly mixture formations for each cylinder in a transient state (Table 7.1, Figure 7.15). This coefficient indicates the number of cycles after which fuel mass in a cylinder has increased or decreased by 99% of a jump, i.e. it has been close to a target value. It should be noted that the value of Lc(99) was determined using the model with the identified parameters γ and τ.

Table 7.1. Values of $L_{c(99)}$ coefficient

	Increase						Decrease							$\overline{L}_{c(99)}$	σ_{Lc}
Cylinder number	1	2	4	5	6	average	1	2	3	4	5	6	average		
1	38	35	37	50	50	42,0	33	34	39	29	33	35	33,8	37,9	6,42
2	31	37	32	27	39	33,2	48	32	37	29	25	28	33,2	33,2	6,32
3	22	29	33	28	33	29,0	38	44	38	29	29	32	35,0	32,0	5,72
4	30	32	39	40	37	35,6	62	40	46	36	31	38	42,2	38,9	8,46
5	24	32	30	24	38	29,6	24	26	33	34	32	32	30,2	29,9	4,52
6	27	22	25	27	27	25,6	45	36	39	25	23	31	33,2	29,4	6,96
7	32	28	25	19	26	26,0	26	19	19	30	24	34	25,3	25,7	4,96
8	24	17	21	25	20	21,4	40	21	28	31	38	30	31,3	26,4	7,07
9	43	25	32	41	24	33,0	30	38	44	36	37	38	37,2	35,1	6,45

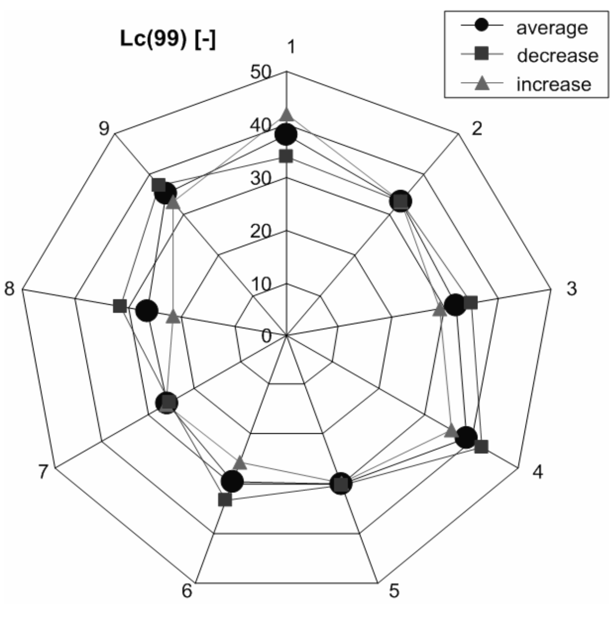

Fig. 7.15. Distribution of the values of $L_{c(99)}$ for each cylinder in a radial engine

If the geometric orientation of inlet pipes in a radial engine influences mixture formation, it will vary mixture composition in each cylinder after a rapid change in injection time. This will follow the varied courses of fuel transportation from an injector cross section into an intake valve cross section. The said hypothesis can be verified if the number of the cycles that must pass between an injection time jump and reaching a steady state is assumed to measure composition diversity, i.e. $L_{c(99)}$ is assumed to be a measure of the dynamics of mixture formation.

If two different cylinders have two different values of $L_{c(99)}$, the hypothesis can be proven as follows. It was assumed that the distribution of $L_{c(99)}$ is normal, which allows a classical statistical theory to be used. A significance level α was determined for the experimental $\overline{L}_{c(99)n1}$, σ_{Lcn1}, N_{n1} I $\overline{L}_{c(99)n2}$, σ_{Lcn2}, N_{n2} are given in Table 7.2. The indices of n1 and n2 stand for the selected numbers of cylinders to be compared. According to the theory of statistics, the α values obtained can be divided into four ranges:

$\alpha > 0{,}10$ - the difference is statistically insignificant,
$0{,}10 \geq \alpha > 0{,}05$ - the difference is negligible,
$0{,}05 \geq \alpha > 0{,}01$ - the difference is significant,
$0{,}01 > \alpha$ - the difference is highly significant.

Table 11 provides the results of the statistical analysis that compared all the cylinders in relation to the parameter. The values from each a significance level were highlighted to mark its scope.

Table 7.2. Significance level of the differences for the mean value of $L_{c(99)}$

Nr cylindra	1	2	3	4	5	6	7	8	9
1		0,1412	0,0667	0,6313	**0,0060**	0,0167	**0,0002**	**0,0020**	0,4389
2	0,1412		0,7395	0,0876	0,1980	0,2588	**0,0076**	0,0465	0,4727
3	0,0667	0,7395		**0,0450**	0,3177	0,3821	**0,0118**	**0,0724**	0,2844
4	0,6313	0,0876	**0,0450**		**0,0062**	**0,0129**	**0,0003**	**0,0020**	0,2591
5	**0,0060**	0,1980	0,3177	**0,0062**		0,9454	0,0577	0,2578	**0,0438**
6	0,0167	0,2588	0,3821	**0,0129**	0,9454		0,1456	0,3647	0,0794
7	**0,0002**	**0,0076**	**0,0118**	**0,0003**	0,0577	0,1456		0,6698	**0,0013**
8	**0,0020**	0,0465	**0,0724**	**0,0020**	0,2578	0,3647	0,6698		**0,0112**
9	0,4389	0,4727	0,2844	0,2591	**0,0438**	0,0794	**0,0013**	**0,0112**	

The results obtained make very clear that the geometric orientation of a cylinder and intake pipe influences the dynamics of mixture formation. Most importantly, there are no random deviations from the average, i.e. it is easy to note that the time constant of the entire groups of cylinders that are close to each other increases or decreases. The time constant for the upper cylinders (9, 1, 2) increased significantly. This means that mixture formation is influenced by the factors related to the angle between a cylinder axis and the vertical. Shifting the axis indicating the cylinders that slowly react for a jump-like fuel dose from the vertical means the impact of factors other than gravity, i.e. these are probably the factors associated with the mass forces of air stream. Their detailed investigation is a future study that requires expanding measurement apparatus by sensors to measure the distribution of film thickness along an inlet pipe.

7.4 Injection time control algorithm

Fuel injection control algorithm is run in a controlling computer with a frequency compatible with engine speed. During each crankshaft rotation, a fuel dose of half a cylinder is injected into individual pipes. Thus, all the needed dose of gasoline is injected in one cycle that lasts two shafts. The input data for the injection time control algorithm are:

a) the rotational speed *n(t)*, pressure in the inlet system $p_d(t)$, intake air temperature $T_d(t)$, fuel temperature $T_{pal}(t)$, fuel pressure $p_{pal}(t)$, head temperature $T_{gl}(t)$ and installation voltage $U_A(t)$ measured at time t
b) the previous values of the estimated fuel mass $m_{cyl,i}(t\text{-}\Delta t)$ in *i*-time cylinders at the time *(t - Δt)*,
c) the values of the τ_i time constant of a fuel film loss in *i*-time cylinder.

Based on the measured rotational speed *n(t)*, the interval between successive injections is calculated:

$$\Delta t = \frac{60}{n(t)[rpm]}[s] \tag{7.1}$$

Then, there are strategic calculations that determine the inflicted value of an excess air ratio:

$$\lambda_{zad}(t) = f_\lambda[n(t), p_d(t), p_{pal}(t), T_{gl}(t)]. \tag{7.2}$$

The next step is to define the mass of air in the cylinders:

$$m_{pow}(t) = f_{pow}[p_d(t), T_{gl}(t), n(t)]. \tag{7.3}$$

Later, the mass of fuel in the cylinder is calculated:

$$m_{cyl}(t) = \frac{m_{pow}(t)}{L_t \cdot \lambda_{zad}(t)}, \tag{7.4}$$

where Lt is the theoretical demand for air in combustion. The most important part of the algorithm is to calculate the mass injection for *i*-time cylinder:

$$m_{wtr}(t,i) = \frac{1}{2}\left\{\frac{\tau(i)}{\Delta t}\left[m_{cyl}(t,i) - m_{cyl}(t-\Delta t, i)\right] + m_{cyl}(t,i)\right\}, \tag{7.5}$$

$i = 1\ldots9$.

The calculated value of injection mass is converted to injector opening time with the correction of fuel temperature and supply voltage:

$$t_{wtr}(t,i) = f_{wtr}\left[m_{wtr}(t,i), T_{pal}(t), U_A(t)\right]. \tag{7.6}$$

The first computational step in the algorithm assumes a zero value of the previous injections.

8. Summary

Based on the analysis of the literature, the following conclusions can be drawn:

- the phenomenon of fuel film was accurately described in terms of the impacts of factors such as fuel temperature, air pressure, air flow rate,
- there is no research into the impact of the spatial orientation of intake pipes on how fuel film behaves,
- the model research the author of this monograph conducted with the use of CFD confirm that gravity influences fuel film significantly,
- radial engines show a great diversity of head temperature, exhaust gas temperature and maximum pressure due to the diversity of individual cylinder mixture composition,
- a multi-point fuel injection system improves the uniformity of supplying cylinders in a radial engine,
- a dose of fuel injected into inlet pipes needs to be varied to enhance the uniformity of the working process of each cylinder in a radial engine.

The studies allowed the author to estimate how the position of cylinders influences the variability of the mixture formation in the radial engine. The minimum value of a significance level in the case of the mean $L_{c(99)}$ coefficient for cylinders 1 and 7 is 0.0002.

The objective has been achieved and the injection time control algorithm for the radial engine injectors that work in a transient state allows for varied mixture formation in individual cylinders.

The main research objective of this monograph was to decide how important the varied mixture formation in each cylinder in a radial engine can be. During the bench test, many interesting phenomena were noted both when the injection system was developed and when the identification test was done. The author did not provide the results attained as he focused only on proving the said hypothesis. However, certain observations and conclusions on how to verify the injection system in relation to the assumed precision of injectors are given below. In other words, the author emphasizes that the varied mixture composition in each cylinder in a transient state was due to the varied mixture formation and the loss of fuel film but not the inaccurate dosing of fuel by individual injectors.

1. The mass of the accumulated fuel that filled the torus and pipes was about 9000 times higher than the injection mass. Thus, the effect of the instantaneous pressure drop in the fuel rail after the next injection does not change much the fuel pressure in the torus.
2. The components of the fuel system such as an electric fuel pump, a mechanical fuel pump, a pressure regulator and fuel filters have been

selected to cause no disorders that could result in the significant variations of individual injections.

3. The verification tests to determine the degree of injectors uniqueness showed that the differentiation of expenditure per injector was less than 1%. In addition, the assumed research scope focused on the dynamic tests, which meant that even small variations of individual injectors would not affect specifying the time lag to reach a steady state.
4. Undoubtedly, the dynamics of the mixture formation depends on the way the injectors are mounted in inlet pipes. If the angle between installed injectors and an inlet pipe axis or the distance between injectors and engine heads changed, the mixture formation in a radial engine would change vitally. The analysis of mechanical and thermal loads has confirmed the place and way the injectors were installed. Changing the geometry of the injectors installation or a type of injectors will require in each case the parameters of mixture formation to be specified again.
5. A testing needs to be repeated in the case of a different type of fuel, e.g. automotive gasoline or an automotive gasoline-and-ethanol mixture.
6. The use of the injection system and consequently the programmable control unit enables to adapt mixture composition to engine operating conditions. Consequently, the function of gasoline to cool an engine at maximum (take-off) power can be reduced at a reduced load (cruising power). As a result, fuel consumption is reduced by 18%, which would be impossible with the use of a carburetor system.
7. The detailed injection control algorithm has procedures that make injection time dependent on such factors as the temperature and air pressure in an inlet system, fuel temperature, head temperature, crankshaft rotational speed, throttle position or installation voltage. If these factors occur, the mixture formation responds to the geometry of inlet pipes and cylinders in a different way. The dependence of the parameters that characterize mixture formation (γ and τ) should be examined in the future. Such research should be conducted in a laboratory the engine manufacturer does not have at pre-sent. In particular, it is impossible to change air supply and, due to air cooling, to control engine temperature in the test bench.
8. Any further studies that lead to a more detailed description of the mixture formation in a radial engine including the impact of other factors are planned as the author's future research work.
9. Simulation research should be important in the future studies, especially in relation to the way fuel is transported in intake pipes.

References

[1] Aquino C. F.: Transient A/F Control Characteristics of the 5 Liter Central Fuel Injection Engine. SAE Technical Paper No. 810494, 1981.

[2] Behnia M., Milton B. E.: Fundamentals of fuel film formation and motion in SI engine induction systems. Energy Conversion and Management, No. 42/15-17, 2001, pp. 1751–1768.

[3] Benninger N., Plapp G.: Requirements and Performance of Engine Management Systems under Transient Conditions. SAE Technical Paper No. 910083, 1991, pp. 118-127.

[4] Berckũller M., Tail N. P., Greenhalgh D. A.: The influence of local fuel concentration on cyclic variability of a lean burn stratified-charge engine. SAE Technical Paper No. 970826, 1997.

[5] Brehob D., Newman C.: Monte Carlo Simulation of Cycle-to-Cycle Variability. SAE Technical Paper No. 922165, 1992.

[6] Brown C., Ladommatos N.: A numerical study of fuel evaporation and transportation in the intake manifold of a port-injected spark-ignition engine. Proceedings of the Institution of Mechanical Engineers, Vol. 205, 1991, pp. 161-175.

[7] Carryer J., Roy R., Powell J.: Estimating in-cylinder pre-combustion mixture temperatures using acoustic resonances. Advanced Automotive Technologies - American Society of Mechanical Engineers, Vol. 40, 1991, pp. 127-138.

[8] Chauvin J., Moulin P., Corde G., Petit N., Rouchon P.: Real-time nonlinear individual cylinder air fuel ratio observer on a diesel engine test bench. IFAC, 2005.

[9] Czarnigowski J., Wendeker M., Jakliński P., Pietrykowski K., Nazarewicz A., Gęca M., Zyska T.: Testing non-uniformity of the combustion process in a radial aircraft engine. SAE Technical Paper No. 2007-01-2074, 2007.

[10] Davis G. W., Ego A., Baumbach S., Jordan C., Bong E.: The determination of air/fuel ratio differences between cylinders in a production engine using exhaust gas oxygen sensors. SAE Technical Paper No. 1999-01-1170, 1999.

[11] Drallmeier J. A.: Hydrocarbon-vapor measurements in pulsed fuel sprays. Appl. Optics, No. 33/33, 1994, pp. 7781–7788.

[12] Durst F., Fukui K., Pereira J. C. F.: Fluid dynamically caused cycle-to-cycle variations in piston-driven pipe expansion flows. Experiments in Fluids, Vol. 13, Issue 1, 1992, pp. 1-10.

[13] Filipek P., Kamiński T., Mitraszewska I., Nowacki G., Wendeker M., Wojciechowski A.: Rozwój układu pomiaru jonizacji w komorze

spalania silnika o zapłonie iskrowym, Journal of KONES, Powertrain and Transport, 2006, Vol. 13, No. 4, pp. 147-154.

[14] Fry M., Nightingale C., Richardson S.: High-speed photography and image analysis techniques applied to study droplet motion within the porting and cylinder of a 4-valve engine. SAE Paper No. 952525, 1995.

[15] Gissinger G., Renard R., Hassendforder M.: Model Based Design and Control of Diesel Engines. SAE Technical Paper No. 910568, 1991, pp. 1-12.

[16] Hamaia K., Kawajiria H., Ishizukaa T., Nakai M.: Combustion fluctuation mechanism involving cycle-to-cycle spark ignition variation due to gas flow motion in S.I. Engines. Symposium (International) on Combustion, Vol. 21, Issue 1, 1988, pp. 505-512.

[17] Hasson D. A., Flint W. L.: An investigation of the liquid petrol wall film in the manifold of a carburetted spark ignition engine effect of carburettor and manifold geometry on wall film quantities, engine performance and emission. Proc. Inst. Mech. Eng., No. 203D, 1989, pp. 77–89.

[18] Haussner M. i inni: Pressure-measuring glow plug. United States Patent No. 7228730, 2007.

[19] Hayashi S., Sawa N.: A study on the transient characteristics of small IC engines. JSME No. 27/224, 1984, pp. 248–254.

[20] Hendricks E., Sorenson S.C.: SI Engine Controls and Mean Value Engine Modelling. SAE Technical Paper No. 910258, 1991.

[21] Heywood J.B.: Internal Combustion Engine Fundamentals, MCGraw-Hill Science Engineering, 1988.

[22] Hinzea P. C., Cheng W. K. Assessing the factors affecting SI engine cycle-to-cycle variations at idle. Symposium (International) on Combustion, Vol. 27, Issue 2, 1998, pp. 2119-2125.

[23] Hires S., Overington M.: Transient Mixture Strength Excursions-An Investigation of Their Causes and Development of a Constant Mixture Strength Fuelling Strategy. SAE Technical Paper No. 810495, 1981.

[24] Hohsho Y., Kanno K., Nakai H., Kadota T.: Characteristics of response of carburetted SI engine under transient conditions. Biull. JSME No. 28/242, 1985, pp. 1725–1732.

[25] Houben H., Marto A., Penchhold F., Hussner M. Borgers M.: Pressure sensor glow plug (psg) for diesel engines. MTZ Worldwide, Vol. 65, 2004.

[26] Ishii K., Sasaki T., Urata Y., Yoshida K., Ohno T.: Investigation of cyclic variation of IMEP under lean burn operation in spark-ignition engine. SAE Technical Paper No. 972830, 1997.

[27] Kroetz, G., Wondrak, W., Obermeier, E., Cavalloni, C.: Silicon carbide on silicon-an ideal material combination for harshenvironment sensor applications. IEEE 0-7803-4756-0, pp. 732-736.

[28] Ladommatos N.: Mechanisms of heat transfer to liquid films in the manifold of port-injected petrol engines. Proceedings of the Institution of Mechanical Engineers, Vol. 207, 1993, pp. 211-221.

[29] Ladommatos N., Rose D.: Monitoring of the mexture strenght in the cylinders of a port-injected gasoline engine during transient operation. Proceedings of the Institution of Mechanical Engineers, Vol. 209, 1995, pp. 127-134.

[30] Lan H., Friedrich M., Armaly B.F., Drallmeier J.A.: Simulation and measurement of 3D shear-driven thin liquid film flow in a duct. International Journal of Heat and Fluid Flow Vol. 29, Issue 2, 2008, pp. 449-459.

[31] Lee C. F., Cheng W. L., Wang D.: Finite diffusion wall film evaporation model for engine simulations using continuous thermodynamics. Proceedings of the Combustion Institute 32/2, 2009, pp. 2801-2808.

[32] Milton B.E., Behnia M., Chen P.Y.P., Blakeley M.R.: Simulation of fuel film formation in ducts. Finite Elements in Analysis and Design Vol. 18, Issues 1-3, 1994, pp. 349-363.

[33] Moskwa J.: Estimation of Dynamic Fuel Parameters in Automotive Engines. Journal of Dynamic Systems, Measurement and Control, Vol. 116, December 1994, pp. 774-780.

[34] Moudden Y.: Extraction of peak pressure position information from the spark-plug ionization signal. Computer Standards & Interfaces Vol. 24, Issue 2, 2002, pp. 161-170.

[35] Moulin P., Corde G., Chauvin J., Castagné M.: Cylinder individual AFR estimation based on a physical model and using Kalman filters. SAE Technical Paper No. 2004-01- 422, 2004.

[36] Ohashi Y., Fukui W., Ueda A.: Application of Vehicle Equipped Ionic Current Detection system for the Engine Management System. SAE Technical Paper No. 970031, 1997.

[37] Ozdor N., Dulger M., Sher E.: An Experimental Study of the Cycle Variability in Spark Ignition Engines. SAE Technical Paper No. 960611, 1996.

[38] Patrick R., Powell J.: Technique for the real-time estimation of air-fuel ratio using molecular weight ratios. SAE Transactions Sect. 3, 1990, pp. 686-698.

[39] Pfahl U., Adomeit G.: Self-Ignition of Diesel-Engine Model Fuels At High Pressures, SAE Technical Paper No. 970897, 1997.

[40] Piernikarski D., Hunicz J.: Investigation of Misfire Nature Using Optical Combustion Sensor in a SI Automotive Engine. SAE Technical Paper No. 2000-01-0549, 2000.

[41] Piernikarski D., Wendeker M.: Experimental stand for optical fiber combustion sensing in a spark ignition automotive engine. Technology and Applications of Light Guides, Proceedings of International Society for Optical Engineering, Waszyngton, USA, 1997, Vol. 3189, pp. 90-99.

[42] Rivara N., Dickinson P.B. and Shenton A.T.: A transient virtual-AFR sensor using the in-cylinder ion current signal. Mechanical Systems and Signal Processing, Vol. 23, Issue 5, 2009, pp. 1672-1682.

[43] Roberts J.B., Peyton-Jones J.C., Landsborough K.J.: Cylinder Pressure Variations as a Stochastic Process. SAE Technical Paper No. 9970059, 1997.

[44] Rychter T., Teodorczyk A.: Modelowanie matematyczne roboczego cyklu silnika tłokowego. PWN, Warszawa 1990.

[45] Sekozawa T., Takahashi S., Shioya M., Ishii T., Asano S.: Development of a Highly Accurate Air-Fuel Ratio Control Method Based on Internal State Estimation. SAE Technical Paper No. 920290, 1992, pp. 19-25.

[46] Senda J., Al-Roub M., Farrell P., Kanda T., Fujimoto H.: Modeling Spray Impingement Considering Fuel Film Formation on the Wall. SAE Technical Paper No. 970047, 1997.

[47] Senda J., Ohnishi M., Fujimoto H. Utsunomiya A.: Estimation of Wall Fuel Film in Port-Injected Engine. Part 1 Modeling of Fuel Film Formation process. Biryuka Shinpojiumu Koen Ronbunshu Vol.7, 1998, pp. 85-90.

[48] Shayler P.J., Teo Y.C., Scarisbrick A.: Determining fuel transfer characteristics for mixture control during transient operation. IMech. E. C469/008, 1993, pp. 81–87.

[49] Simon S.: Fuel injection valve and pressure sensor combination. United States Patent No. 6318342, 2000.

[50] Sohma K., Yukitake T., Azuhata S., Takaku Y.: Application of Rapid Optical Measurement to Detect the Fluctuations of the Air-Fuel Ratio and Temperature of a Spark Ignition Engine. SAE Technical Paper No. 910499, 1991, pp. 806-812.

[51] Spathopoulou M., Gavaises M., Theodorakakos A., Yanagihara H.: Formation and development of wall liquid films during impaction of gasoline fuel sprays. Atomizations and Sprays Vol.19, Issue 8, 2009.

[52] Stanton, D., C. Rutland: Modeling Fuel Film Formation and Wall Interaction in Diesel Engines. SAE Technical Paper No. 960628, 1996, pp. 808-824.

[53] Stanton D., Rutland C. J.: Multi-dimensional modeling of heat and mass transfer of fuel films resulting from impinging sprays. SAE Technical Paper No. 980132, 1998.

[54] Sung N. W., Choi J. S., Jeong Y. I.: A Study on the Flow in the Engine Intake System. SAE Technical Paper No. 952067, 1995.

[55] Tanaka M, Durbin EJ.: Transient Response of a Carburator Engine. SAE Technical Paper No. 770046, 1978.

[56] Wang D. Y., Detwiler E.: Exhaust oxygen sensor dynamic study. Sensors and Actuators B: Chemical, Vol. 120, Issue 1, 2006, pp. 200-206.

[57] Watarai, T., Nakashima F., Hiramatsu H.: Combustion pressure sensor designed to ensure stability of output characteristic and sensitivity. United States Patent No. 6973820, 2005.

[58] Wendeker M.: Experimental Results of the Investigation of the Mixture Preparation. SAE Technical Paper No. 98456, 1998.

[59] Wendeker M.: Sterowanie napełnianiem w silniku samochodowym. LTN, Lublin 1999.

[60] Wendeker M.: Sterowanie wtryskiem benzyny w silniku samochodowym. LTN, Lublin 1999.

[61] Wendeker M., Jakliński P., Czarnigowski J., Filipek P.: Investigation of the wideband SI lambda controlling system. Journal of KONES: Internal Combustion Engines, 2002, Vol. 9, 3-4, pp. 292-298.

[62] Wendeker M., Kamiński T.: Development of a fiber-optic sensor for the measurement of dynamic cylinder pressure in spark ignition engine. IEEE 0-7803-4756-0, 2005, ss. 1-8.

[63] Wiedenmann H., Raff L., Noack R.: Heated Zirconia Oxygen Sensor for Stoichiometric and Lean Air-Fuel Ratios. SAE Technical Paper No. 840141, 1984, pp. 1843-1847.

[64] Williams P, Beckwith P.: The Effect of Fuel Composition and Manifold Conditions Upon Spray Formation From An SI Engine Pintle Injector. SAE Technical Paper No. 941865, 1994.

[65] Włodarczyk M. T.: Glow plug integrated pressure sensor. United States Patent No. 7207214, 2005.

[66] Włodarczyk M. T., Poorman T. J.: Temperature compensated fiber-optic pressure sensor. United States Patent No. 6823738, 2003.

[67] Wright J.H., Drallmeier J.A.: Cyclic variability of pulsed spray vapor fields. Experiments in Fluids 25, 1998, pp. 329–336.

[68] WSK PZL – Kalisz: Opis techniczny silnika lotniczego K9-AA i K9-BB. WT-K9A.00.01, Kalisz 1990.

[69] Yorita H., Miwa T., Hiramatsu H.: Combustion chamber pressure sensor equipped with damper body for attenuating transmitted engine vibration. United States Patent No. 7313949, 2005.

[70] Yoshikawa, Y., Nakada, T., Itoh, T., Takagi, Y.: Numerical Simulation System for Analyzing Fuel Film Flow in Gasoline Engine. SAE Technical Paper No. 930326, 1993.

[71] Zervas E.: Correlations between cycle-to-cycle variations and combustion parameters of a spark ignition engine. Applied Thermal Engineering, Vol.24, Issues 14-15, 2004, pp. 2073–2081.

[72] Zhang L., Ueda T., Takatsuki T., Yokota K.: Cycle-to-cycle variation of cylinder flow in a motored engine. JSME Int. J. B 38 3, 1995, pp. 426–431.

[73] Zhao F., Kadota T., Takemoto T.: Temporal and Cyclic Fluctuation of Fuel Vapour Concetration in a Spark Ignition Engine. SAE Technical Paper No. 912346, 1991, pp. 1761-1776.

Websites:

[74] http://www.beru.com/english/produkte/psg.php

[75] http://www.cd-adapco.com/about/what-is-cfd.html

[76] http://www.cd-adapco.com/products/STAR-CD/performance/320/index.html

[77] http://www.intertechnology.com/Kistler/pdfs/Pressure_Model_6061B.pdf

[78] http://www.radialengines.com/fuel_injection/index.htm